

Distribution-Free Selection of Low-Risk Oncology Patients for Survival Beyond a Time Horizon

Matteo Sesia

SESSIA@MARSHALL.USC.EDU

University of Southern California

Departments of Data Sciences and Operations, and of Computer Science

Los Angeles, California, USA

Vladimir Svetnik

VLADIMIR_SVETNIK@MERCK.COM

Merck & Co., Inc.

Rahway, New Jersey, USA

Abstract

We study the problem of selecting a subset of patients who are unlikely to experience an event within a specified time horizon, by calibrating a screening rule based on the output of a black-box survival model. This statistics problem has many applications in medicine, including identifying candidates for treatment de-escalation and prioritizing the allocation of limited medical resources. In this paper, we compare two families of methods that can provide different types of distribution-free guarantees for this task: (i) high-probability risk control and (ii) expectation-based false discovery rate control using conformal p -values. We clarify the relation between these two frameworks, which have important conceptual differences, and explain how each can be adapted to analyze time-to-event data using inverse probability of censoring weighting. Through experiments on semi-synthetic and real oncology data from the Flatiron Health Research Database, we find that both approaches often achieve the desired survival rate among selected patients, but with distinct efficiency profiles. The conformal method tends to be more powerful, whereas high-probability risk control offers stronger guarantees at the cost of some additional conservativeness. Finally, we provide practical guidance on implementation and parameter tuning.

Keywords: Survival analysis; censored data; conformal inference; false discovery rate; multiple testing; selective inference; machine learning.

1 Introduction

1.1 Background and Motivation

A common statistical problem in oncology care is to identify a subset of low-risk patients who are sufficiently unlikely to experience an adverse event within a fixed time horizon. This problem has many applications, including determining eligibility for less intensive management strategies such as active surveillance instead of surgery, and optimizing the allocation of limited resources to patients most likely to benefit. For example, consider a phase II de-escalation study that aims to enroll only patients who are sufficiently low risk, with a protocol target of no more than 10% event probability within 3 months among participants. This means that approximately 90% of enrolled patients should remain event-free for at least 3 months. Ensuring the screening protocol is properly calibrated is often essential in practice: a screening rule that is more liberal than expected may raise safety

issues, possibly prompting early termination of the study, while an overly conservative one may exclude too many eligible patients, resulting in an inefficient, low-yield study.

Patient screening is nowadays typically data-driven, guided by survival probabilities estimated by potentially complex models that factor diverse patient characteristics, including rich demographic information and clinical histories. A wide range of models are available to estimate survival probabilities. Classical covariate-based approaches include parametric models (e.g., exponential or Weibull) and the semi-parametric Cox proportional hazards model (Cox, 1972). In large-scale datasets with high-dimensional covariates, more flexible machine-learning approaches (Bertsimas and Wiberg, 2020)—such as random survival forests (Ishwaran et al., 2008), deep neural networks (Katzman et al., 2018), or gradient-boosting models (Barnwal et al., 2022)—are often more effective for discriminating between lower- and higher-risk patients. However, all models have limitations: classical survival models rely on assumptions that may be difficult to verify in practice (e.g., parametric forms or proportional hazards), whereas machine-learning approaches are typically not designed to provide statistical guarantees. Therefore, it is not straightforward to extract well-calibrated screening rules from models used in practice.

To address this challenge, we study flexible calibration methods that can provide statistical guarantees on the future event rate within a subset of patients selected using the output of any survival model. To ensure broad applicability, we focus on *distribution-free* and *model-agnostic* methods that do not rely on simplifying assumptions on the population distribution or the internal structure of the predictive model. The goal of this paper is primarily integrative and comparative: rather than proposing a new inferential framework, we demonstrate how two recent lines of research from the statistics and machine learning literature—namely, fixed-sequence high-probability control (Bauer, 1991; Angelopoulos et al., 2025) and conformal prediction (Vovk et al., 2005; Angelopoulos and Bates, 2023)—can be adapted to this survival analysis problem, where one must account for the presence of censored data. We clarify their conceptual relation, highlight their strengths and limitations, and compare them with simpler approaches based on pointwise and uniform confidence intervals. Finally, we provide practical guidance for applying these methods effectively.

1.2 Problem Preview: Data-Driven Calibration Under Right-Censoring

Consider a model-based estimate of the survival probability at time $t_0 > 0$ for a patient with covariates X , denoted by $\hat{S}(t_0 | X) \in [0, 1]$. This estimate may come from any survival model. A prototypical low-risk screening rule selects patients whose estimated survival probability is sufficiently high, that is, those with features X such that $\hat{S}(t_0 | X) \geq \lambda$, where $\lambda \in [0, 1]$ is a (potentially data-driven) threshold parameter that defines the rule. At a high level, our goal is to determine a suitable value of λ that ensures the screening rule is well-calibrated for a target event probability $\alpha \in [0, 1]$ (for example, $\alpha = 0.1$), so that the true event rate among selected patients is approximately equal to α .

A model-agnostic way to tune λ is to use an independent calibration dataset, not used to fit the model: apply the screening rule with different candidate values of λ to the calibration data, estimate the corresponding survival rates among selected patients, and then choose the value of λ whose empirical survival rate best matches the desired target. As long as

this evaluation is performed on independent data, it provides an unbiased assessment of the realized event rate at test time even if the survival model itself is misspecified or overfit.

While this idea is intuitive, there are two technical challenges. The first challenge is that survival data are often right-censored, meaning that for many patients in the calibration set the event status by time t_0 is unknown, which complicates direct estimation of event rates. The second challenge is that tuning λ by comparing empirical event rates across multiple candidate thresholds introduces a delicate multiple testing problem. As we evaluate several λ values and select the one whose observed performance most closely matches the target, we are using the same calibration data for two distinct purposes: estimating the event rate at each threshold and optimizing the threshold itself—in statistical terms, this constitutes “double dipping”. If not handled carefully, this complication could lead to miscalibrated screening rules because the apparent event rate at the chosen, data-dependent threshold λ may deviate from the true population event rate more than would be expected by chance for any fixed value of λ .

The first challenge, censoring, has a well-established remedy: inverse probability of censoring weighting (IPCW) (Robins and Rotnitzky, 1992; Robins, 1993; Vock et al., 2016). In its simplest implementation, IPCW reweights the uncensored observations in the calibration set by the inverse of the estimated probability of remaining uncensored up to the relevant time (e.g., t_0 or the observed event time). This approach yields consistent estimates of time-dependent error rates under standard assumptions on the censoring mechanism and, through large-sample approximations such as the delta method (Uno et al., 2007) or the bootstrap (Beyene et al., 2024), enables the construction of asymptotically valid confidence intervals for the true event rate corresponding to any fixed selection threshold λ .

The second challenge, multiple testing over λ , represents the primary focus of this paper. A straightforward but unsatisfactory approach is to randomly split the calibration dataset into two disjoint subsets, using one to estimate event rates and select the optimal threshold, and the other to validate the chosen threshold by re-estimating its corresponding event rate, to ensure it meets the desired standard (e.g., being confidently lower than 10%). However, this strategy is data-intensive and potentially unreliable in limited samples: in practice, the selected threshold may fail the validation check, necessitating repeated iterations of this procedure using new independent data. An alternative approach based on classical statistical ideas is to use a single calibration set to construct simultaneous (uniform) confidence bands for the selected-set event rate across a range of candidate λ values, for example using Bonferroni adjustments or Gaussian multiplier/perturbation bootstrap methods (Park and Wei, 2003; Zheng et al., 2008, 2010; Fleming and Harrington, 2013). Unfortunately, uniform inference is often very conservative in practice, as we will demonstrate empirically. This motivates the need for new approaches.

Recent developments in the statistics and machine learning literature have produced more efficient inference tools that can be applied to calibrate the output of *any model* using a single held-out dataset; e.g., see Angelopoulos and Bates (2023) for an introductory review of this broader field. Although initially developed for i.i.d. settings with fully observed data, it has been shown that these methods can also handle censored data using different techniques, including covariate shift re-weighting (Candès et al., 2023; Gui et al., 2024) and IPCW (Farina et al., 2025; Sesia and Svetnik, 2025b). Specifically, there are two classes of modern distribution-free inference approaches that are applicable to our problem: one based

on *fixed-sequence testing* (Bauer, 1991) instantiated through the *Learn–Then–Test* (LTT) framework (Angelopoulos et al., 2024a, 2025), and one based on *conformal prediction* (Vovk et al., 2005; Lei et al., 2018; Angelopoulos et al., 2024b).

The LTT approach takes an estimation-oriented perspective. It prescribes an ordered sequence of candidate thresholds for the screening rule *a priori* (for example, starting from a clinically motivated guess) and evaluates them sequentially using one-sided IPCW upper confidence bounds for the corresponding event rate, stopping at the first threshold whose confidence upper bound fails to remain below the desired target. This yields a clean safety guarantee while typically being far less conservative compared to calibration based on uniform confidence bands. However, one limitation is that it can be challenging in practice to choose a good value for the confidence level of the IPCW bounds. As we will show, higher confidence levels tend to produce overly conservative screening rules, whereas lower confidence levels result in harder-to-interpret guarantees and less stable selections.

Conformal prediction offers an alternative approach that can produce similarly rigorous, although somewhat different, statistical guarantees without the added complication of requiring confidence level pre-specification. Intuitively, the conformal approach treats each patient-level selection as a hypothesis test and computes a corresponding *conformal p-value* (Jin and Candès, 2023), where the null hypothesis is that the patient will not experience the event before time t_0 . Selected patients are then viewed as “discoveries”, and those among them who experience the event before t_0 constitute “false discoveries”. Applying the Benjamini-Hochberg (BH) procedure (Benjamini and Hochberg, 1995) to these conformal *p*-values approximately controls the False Discovery Rate (FDR), and thus this approach leads to the selection of a subset of patients for whom the event rate is guaranteed to fall below the specified threshold *in expectation* (Sesia and Svetnik, 2025b).

We will show that the conformal method often performs well in practice, yielding selection rules that are both efficient and well-calibrated. However, we will also see that its theoretical guarantees have a different, somewhat weaker interpretation than those given by the LTT approach, especially if selections are very rare. Indeed, these FDR guarantees cannot be directly expressed as statements about the calibration of an *inductive* screening rule of the form $\hat{S}(t_0 | X) \geq \hat{\lambda}$, where $\hat{\lambda}$ depends solely on the calibration data. Instead, they produce *transductive* screening rules in which the effective threshold $\hat{\lambda}$ depends also on the features of all patients in the test dataset.

After reviewing related work and formalizing the problem, we will delineate the conceptual differences between these two methods in more detail, describe their implementations for censored data (via IPCW), and compare them empirically against more classical approaches based on pointwise and simultaneous IPCW inference.

1.3 Related Works and Contributions

This paper builds upon a rich and rapidly growing literature on distribution-free inference and conformal prediction (Vovk et al., 2005); e.g., see Angelopoulos and Bates (2023); Angelopoulos et al. (2024b) and references therein as a starting point for a broad review. This methodology has already found clinical applications (Vazquez and Facelli, 2022; Olsson et al., 2022), including in oncology care (Bergquist et al., 2022). For the analysis of time-to-event data under censoring, conformal prediction techniques have been applied to construct

prediction intervals for survival times—initially under simplified censoring regimes (Candès et al., 2023; Gui et al., 2024), and more recently under general right-censoring using bootstrapping (Qin et al., 2025), IPCW (Farina et al., 2025), or doubly robust adjustments (Davidov et al., 2025; Sesia and Svetnik, 2025a). In this paper, we apply conformal prediction methods to calibrate a cohort screening rule, building upon the framework of Jin and Candès (2023), which combines conformal p -values with FDR control via the BH procedure (Benjamini and Hochberg, 1995). Subsequent extensions of this framework have addressed covariate shift (Jin and Candès, 2025) and right-censoring in time-to-event-data through IPCW (Sesia and Svetnik, 2025b). We adopt the approach of Sesia and Svetnik (2025b) to obtain expectation-level control of the event fraction among selected patients and compare this method to the alternative LTT framework (Angelopoulos et al., 2024a, 2025).

The LTT framework shares with conformal prediction the goal of providing distribution-free uncertainty quantification for black-box machine learning models, but it follows a different perspective. Whereas conformal prediction focuses on *predictive* inference and controls error rates in expectation, LTT adopts an *estimation*-oriented perspective which, in our context, leads to *high-probability* guarantees on the realized risk of the selected subset. To the best of our knowledge, the LTT framework remains relatively under-utilized in the analysis of censored time-to-event data, even though it is easy to apply due to its compatibility with any risk estimators, including IPCW-based approaches.

The problem studied in this paper is related to, but distinct from, time-dependent “receiver operating characteristic” analysis, which aims to quantify how well a prognostic score ranks patients according to their risk of experiencing an event by a given time horizon (Heagerty et al., 2000; Heagerty and Zheng, 2005; Blanche and Blanche, 2013; Yuan et al., 2018). Discrimination metrics such as the “area under the curve” measure overall ranking accuracy but do not ensure that any specific decision threshold corresponds to an acceptable event rate among patients classified as low- or high-risk. In contrast, clinical screening decisions depend on calibration at the operating point—that is, ensuring the event rate among those selected (or unselected) meets a predefined target. This paper addresses this calibration problem directly: rather than evaluating how well a model discriminates across the full range of risk scores, we compare procedures that calibrate a selection rule providing explicit statistical guarantees on the event rate within the subset of selected patients.

2 Preliminaries

2.1 Notation and Problem Statement

For each individual indexed by $i \in \mathbb{N}$, let $X_i \in \mathcal{X} \subseteq \mathbb{R}^d$ denote a vector of d covariates, T_i the event time of interest, and C_i the censoring time, after which the individual is no longer observed. Thus, each subject is represented by the triplet (X_i, T_i, C_i) . We assume the individuals are independent and identically distributed (i.i.d.) samples from an underlying population, whose distribution is unknown. In the following, we will sometimes omit the index i , writing (X, T, C) to denote a generic random sample from this population. A common assumption is that T and C are independent conditional on X ; i.e., $T \perp\!\!\!\perp C | X$.

Event and censoring times are not always jointly observable. Instead, for each individual we observe the covariates X_i together with the right-censored time-to-event data

$$E_i := \mathbb{I}(T_i < C_i) \in \{0, 1\}, \quad \tilde{T}_i := \min(T_i, C_i),$$

where E_i indicates whether the event occurred before censoring, and \tilde{T}_i denotes the observed (possibly censored) time.

Let $S(t \mid x) := \mathbb{P}(T > t \mid X = x)$ denote the conditional survival function, and $G(t \mid x) := \mathbb{P}(C \geq t \mid X = x)$ the corresponding function for the censoring time. Both S and G are unknown population quantities. We assume access to estimates \hat{S} and \hat{G} obtained from given survival and censoring models, respectively, which we treat as “black boxes”. These may correspond to parametric, semi-parametric, or obscure machine-learning models. In practice, the censoring model is typically trained analogously to the survival model, but with the event indicators flipped. The function \hat{S} is used to compute covariate-based scores $\hat{s}(x) \in [0, 1]$ that rank patients by their estimated likelihood of surviving beyond a fixed time horizon $t_0 > 0$, with higher scores corresponding to higher predicted survival. The most direct choice is $\hat{s}(x) = \hat{S}(t_0 \mid x)$. The function \hat{G} will later be used for IPCW inference.

Recall that our goal is to identify a subset of low-risk patients who are sufficiently unlikely to experience an adverse event within the time horizon t_0 . To formalize this, we consider a monotone family of screening rules indexed by a threshold $\lambda \in [0, 1]$:

$$A_\lambda(x) := \mathbb{I}\{\hat{s}(x) > \lambda\}, \quad (1)$$

where $A_\lambda(X_i)$ is the selection indicator for subject i .

Throughout this paper, we treat the scoring function \hat{s} as fixed and focus on calibrating the threshold λ so that the resulting screening rule satisfies the desired clinical criteria, as detailed below. Calibration of λ is performed using an independent calibration dataset

$$\mathcal{D}_{\text{cal}} := \{(X_i, \tilde{T}_i, E_i)\}_{i=1}^n,$$

consisting of n i.i.d. right-censored observations from the target population, assumed independent of the fitted models \hat{S} and \hat{G} . Because the screening threshold will in practice be driven by \mathcal{D}_{cal} , which are random, we denote it by $\hat{\lambda}$ to emphasize its data dependence. When appropriate, we will explicitly specify whether probabilities and expectations are taken conditionally on \mathcal{D}_{cal} or marginally over its sampling distribution.

The problem is to calibrate a threshold $\hat{\lambda}$ that selects as many patients as possible while ensuring that those selected are truly “low-risk” within the specified time horizon t_0 . In other words, we seek the largest selected subset that satisfies a pre-specified constraint on the event rate among those selected. To formalize this idea, we can express calibration as an optimization problem.

Given any (possibly data-dependent) screening rule $A : \mathcal{X} \rightarrow \{0, 1\}$, we define the *selected-set risk* at time t_0 (conditional on the calibration data, on which the rule may depend) as

$$r(A; \mathcal{D}_{\text{cal}}) := \mathbb{P}(T \leq t_0 \mid A(X) = 1, \mathcal{D}_{\text{cal}}); \quad (2)$$

that is, the probability that a selected patient experiences the event before t_0 . Similarly, define the marginal probability of selection as

$$\mu(A; \mathcal{D}_{\text{cal}}) := \mathbb{P}(A(X) = 1 \mid \mathcal{D}_{\text{cal}}), \quad (3)$$

which represents the proportion of the population selected as low-risk by the given rule.

The explicit dependence of r and μ on \mathcal{D}_{cal} emphasizes that both quantities are random because the selection rule depends on the data-driven threshold $\hat{\lambda}$ (e.g., $A = A_{\hat{\lambda}}$). For brevity, we sometimes suppress this dependence in notation when it is clear from context.

Given a target survival rate $\alpha \in (0, 1)$, our goal is to calibrate a *data-driven* screening threshold $\hat{\lambda}$, based on the data in \mathcal{D}_{cal} and fixed models trained on $\mathcal{D}_{\text{train}}$, to (approximately) solve the constrained optimization problem

$$\begin{aligned} & \text{maximize}_{\lambda \in [0, 1]} \quad \mu(A_{\lambda}; \mathcal{D}_{\text{cal}}) \\ & \text{subject to} \quad r(A_{\lambda}; \mathcal{D}_{\text{cal}}) \leq \alpha. \end{aligned} \tag{4}$$

In practice, $r(A_{\lambda}; \mathcal{D}_{\text{cal}})$ and $\mu(A_{\lambda}; \mathcal{D}_{\text{cal}})$ must be estimated, and thus the problem can only be solved *approximately*. The remainder of this paper discusses different solution strategies, providing different guarantees and trade-offs between conservativeness and efficiency.

In Section 3, we present methods designed to approximately solve (4) while enforcing the risk constraint with high probability over the randomness in the calibration data. In Section 4, we introduce an alternative approach, grounded in conformal prediction, that seeks to satisfy the risk constraint in expectation. Because both families of methods rely on IPCW to handle right-censoring, we first provide a brief overview of the main ideas underlying IPCW before describing these calibration strategies in detail.

2.2 Handling Censoring with Inverse Probability of Censoring Weighting

Right-censoring complicates the problem because it makes the event status by time t_0 unobserved for some individuals in the calibration dataset. To address this, we rely on the IPCW framework (Robins and Rotnitzky, 1992; Robins, 1993; Vock et al., 2016), a standard approach that enables approximately unbiased estimation of time-dependent quantities—such as event rates or risks—under some assumptions on the censoring mechanism. We provide here a brief overview of the key ideas underlying IPCW; its specific implementation within each calibration method will be described in detail in the following sections.

In essence, IPCW reweights each uncensored individual by the inverse of their estimated probability of remaining uncensored up to the relevant time, $\hat{G}(\bar{T}_i \mid X_i)$, thereby approximating what would have been observed in a fully followed cohort. The validity of IPCW-based inference rests on three assumptions: (i) conditional independent censoring: $T \perp\!\!\!\perp C \mid X$, meaning that, conditional on the covariates X , censoring is uninformative; (ii) positivity: $\inf_{x \in \mathcal{X}, 0 \leq t \leq t_0} G(t \mid x) > 0$, ensuring that every individual has a nonzero probability of remaining uncensored up to the time horizon of interest; (iii) consistent estimation of censoring probabilities: the fitted censoring model $\hat{G}(t \mid x)$, trained on an independent dataset, consistently approximates the true censoring survival function $G(t \mid x)$.

3 Calibration via High-Probability Risk Control

In this section, we present methods to approximately solve the optimization problem in (4) while aiming to satisfy the risk constraint with high probability over the randomness in the calibration data. All these methods are based on constructing confidence intervals for the two key quantities— $r(A_{\lambda}; \mathcal{D}_{\text{cal}})$ and $\mu(A_{\lambda}; \mathcal{D}_{\text{cal}})$ —as functions of the screening threshold $\lambda \in [0, 1]$, using the calibration dataset \mathcal{D}_{cal} . We describe three increasingly refined

approaches: (i) Pointwise calibration, which constructs upper confidence bounds for the risk at fixed values of λ and then selects the most liberal threshold meeting the constraint, ignoring the multiple-testing problem; (ii) Uniform calibration, which employs simultaneous confidence bounds across a grid of λ values to protect against data-dependent threshold tuning, at the cost of increased conservativeness; and (iii) Learn–then–Test (LTT) or fixed-sequence calibration, which performs pointwise estimation sequentially over ordered thresholds, achieving a more practical balance between efficiency and robustness.

3.1 Pointwise Risk Estimation

For any fixed $\lambda \in [0, 1]$, the risk $r(A_\lambda)$ of the screening rule A_λ defined in (1), as given in (2), can be expressed independent of the calibration data \mathcal{D}_{cal} (since λ is fixed) as:

$$r(\lambda) = \frac{\theta(\lambda)}{\mu(\lambda)}, \quad \theta(\lambda) = \mathbb{E}[\mathbb{I}\{T \leq t_0\} A_\lambda(X)], \quad \mu(\lambda) = \mathbb{E}[A_\lambda(X)].$$

Two complementary IPCW estimators are available to estimate these quantities. The first, known as the event-time weighted (IPCW–ET) estimator, upweights observed events before t_0 by the inverse of the estimated probability of remaining uncensored just prior to the event time, $\hat{G}(\tilde{T}_i^- \mid X_i)$. Specifically, it computes the following point estimates:

$$\hat{r}_{\text{et}}(\lambda) = \frac{\hat{\theta}_{\text{et}}(\lambda)}{\hat{\mu}(\lambda)}, \quad \hat{\theta}_{\text{et}}(\lambda) = \frac{1}{n} \sum_{i=1}^n A_\lambda(X_i) \frac{\mathbb{I}(\tilde{T}_i \leq t_0, E_i = 1)}{\hat{G}(\tilde{T}_i^- \mid X_i)}, \quad \hat{\mu}(\lambda) = \frac{1}{n} \sum_{i=1}^n A_\lambda(X_i). \quad (5)$$

This tends to exhibit lower variance when events are relatively frequent before time t_0 , since in that case the numerator $\hat{\theta}_{\text{et}}(\lambda)$ can be estimated from a larger effective sample.

When events are rarer before t_0 , an often preferred alternative is the fixed-time weighted (IPCW–FT) estimator; this upweights individuals known to be event-free at t_0 by the inverse probability of being uncensored at that time, $\hat{G}(t_0 \mid X_i)$. The corresponding estimators are

$$\hat{r}_{\text{ft}}(\lambda) = \frac{\hat{\theta}_{\text{ft}}(\lambda)}{\hat{\mu}(\lambda)}, \quad \hat{\theta}_{\text{ft}}(\lambda) = \hat{\mu}(\lambda) - \frac{1}{n} \sum_{i=1}^n A_\lambda(X_i) \frac{\mathbb{I}(\tilde{T}_i \geq t_0)}{\hat{G}(t_0 \mid X_i)}. \quad (6)$$

In this paper, we primarily adopt the IPCW–ET formulation (5), as it aligns more closely with the conformal prediction method described in Section 4. We also follow the standard practice of applying mild winsorization to the IPCW weights (Cole and Hernán, 2008).

In addition to point estimates of $r(\lambda)$ and $\mu(\lambda)$, in order to calibrate the screening rule we will need a one-sided upper confidence bound (UCB) for $r(\lambda)$, at a prescribed significance level. Let $\delta \in (0, 1)$ denote the significance level, so that a 95% confidence bound corresponds to $\delta = 0.05$. Several approaches are available to construct such bounds.

A common approach that tends to work well in moderate-to-large samples is the delta-method. This approximates $\hat{r}(\lambda)$ as asymptotically Gaussian and computes its large-sample variance using a Taylor expansion, leading to an upper bound of the form

$$\text{UCB}^{\text{pt}}(\lambda; \delta) = \hat{r}(\lambda) + z_{1-\delta} \widehat{\text{SE}}(\hat{r}(\lambda)),$$

where $z_{1-\delta}$ is the $(1 - \delta)$ quantile of the standard normal distribution. We refer to Appendix A1.1 for additional details, including an expression for $\widehat{\text{SE}}(\hat{r}(\lambda))$. An alternative approach with similar characteristics is the nonparametric bootstrap; see Appendix A1.1.2.

When very few patients are selected (e.g., ≤ 10), the asymptotic approximations underlying both the delta-method and bootstrap are no longer justified, requiring instead the use of finite-sample confidence bounds. Finite-sample results have been the main focus of the distribution-free inference literature, including within the LTT framework (Angelopoulos et al., 2024a, 2025), though these estimates are often conservative. In our context, a relatively tight finite-sample upper confidence bound for $r(\lambda)$ can be derived by combining an empirical-Bernstein inequality (Maurer and Pontil, 2009) for the numerator with an exact binomial lower bound for the denominator; see Appendix A1.1.3 for further details.

3.2 Greedy Pointwise Calibration

Given a grid $\Lambda = \{\lambda_1, \dots, \lambda_K\}$ of K candidate thresholds between 0 and 1, the simplest calibration strategy is to compute the estimated risk $\hat{r}(\lambda)$ and a pointwise upper confidence bound for each $\lambda \in \Lambda$ with any of the methods from Section 3.1, then select

$$\hat{\lambda}_{\text{greedy}} \in \arg \max_{\lambda \in \Lambda} \{ \hat{\mu}(\lambda) : \text{UCB}^{\text{pt}}(\lambda; \delta) \leq \alpha \}, \quad (7)$$

where $\hat{\mu}(\lambda) = \frac{1}{n} \sum_{i=1}^n A_\lambda(X_i)$ is the observed selection fraction. Ties, if any, are broken in favor of larger $\hat{\mu}(\lambda)$. Algorithm A2 in Appendix A1 provides a summary of this procedure.

A key limitation of this greedy strategy is that it provides no formal guarantees for the risk of the tuned rule, $r(\hat{\lambda}_{\text{greedy}})$, since pointwise confidence bounds are valid only for pre-specified thresholds. Searching across multiple λ values inflates the chance of selecting one whose UCB is spuriously optimistic: if K candidates are examined, the probability that at least one bound undercovers can increase from δ to as much as $1 - (1 - \delta)^K \approx K\delta$. This problem can be exacerbated by additional, implicit data-driven tuning choices—such as the IPCW formulation, degree of weight stabilization, or grid resolution.

3.3 Conservative Uniform Calibration

One way of ensuring valid inference under data-driven threshold selection is to construct a *uniform* upper confidence bound $\text{UCB}^{\text{unif}}(\lambda; \delta)$ for the risk $r(\lambda)$ satisfying:

$$\mathbb{P} \left[r(\lambda) \leq \text{UCB}^{\text{unif}}(\lambda; \delta), \forall \lambda \in \Lambda \right] \geq 1 - \delta.$$

The calibrated threshold can then be safely selected as

$$\hat{\lambda}_{\text{unif}} \in \arg \max_{\lambda \in \Lambda} \{ \hat{\mu}(\lambda) : \text{UCB}^{\text{unif}}(\lambda; \delta) \leq \alpha \},$$

which ensures $\mathbb{P}[r(\hat{\lambda}_{\text{unif}}) > \alpha] \leq \delta$; see Algorithm A3 in Appendix A1.3.

The simplest approach to obtain uniform confidence bounds applies the pointwise methods from Section 3.1 with a Bonferroni correction, replacing the confidence level δ with $\delta/|\Lambda|$. While straightforward, this tends to be overly conservative (especially when risk estimates are strongly correlated across nearby thresholds) leading to screening rules that are needlessly restrictive. A more efficient alternative is the Gaussian multiplier (perturbation) method, which constructs a joint confidence band by simulating correlated fluctuations in $\hat{r}(\lambda)$ across the grid. This accounts for dependencies between estimates and typically yields tighter bands than Bonferroni when $\hat{r}(\lambda)$ varies smoothly in λ . We refer to Appendix A1.3 for further details on both approaches.

3.4 Learn–Then–Test (LTT) Calibration

We now introduce a third high-probability calibration method that seeks a practical balance between the opposite extremes of the pointwise and uniform approaches presented above: the LTT procedure (Angelopoulos et al., 2024a, 2025), which builds on the idea of *fixed-sequence testing* (Bauer, 1991).

Applying the estimation techniques described in Section 3.1, LTT constructs pointwise upper confidence bounds $UCB^{\text{pt}}(\lambda; \delta_*)$ for the risk $r(\lambda)$ over a grid Λ of candidate thresholds, using a confidence level δ_* defined below. To determine the calibrated threshold $\hat{\lambda}_{\text{LTT}}$, however, LTT does not search greedily over all $\lambda \in \Lambda$ as in (7). Instead, it evaluates whether $UCB^{\text{pt}}(\lambda; \delta_*) \leq \alpha$ sequentially over λ along one or more pre-specified, typically monotone paths through Λ —for instance, decreasing values of λ corresponding to increasingly liberal screening rules—and stops immediately before the first “unsafe” threshold where the risk upper confidence bound exceeds α . When multiple ($L > 1$) paths are considered, the final $\hat{\lambda}_{\text{LTT}}$ is the most liberal (i.e., smallest) among the corresponding stopping points.

This is an instance of fixed-sequence testing (Bauer, 1991), ensuring high-probability risk control without the excessive conservativeness of uniform confidence bounds. Formally, if the risk upper bounds $UCB^{\text{pt}}(\lambda; \delta_*)$ are *pointwise* valid, then $\mathbb{P}[r(\hat{\lambda}_{\text{LTT}}) > \alpha] \leq \delta$. Intuitively, by setting $\delta_* = \delta/L$, LTT operates as if only L candidate thresholds were being tested. The Bonferroni adjustment in $\delta_* = \delta/L$ is typically mild, since a small number of well-designed paths ($L \ll |\Lambda|$) is usually sufficient to find a good calibrated threshold, making LTT substantially less conservative than the approaches described in Section 3.3.

Concretely, we implement LTT using threshold paths defined as follows. We begin by fixing an *anchor* threshold $\lambda_0^{(1)} = 1 - \alpha$, motivated by the intuition that if the survival model \hat{S} is well-calibrated, then $\hat{s}(x) \approx S(t_0 | x)$, so selecting individuals with $\hat{s}(x) \geq \lambda$ should yield an event rate near $1 - \lambda$, implying $r(\lambda_0^{(1)}) \approx \alpha$. Starting from this guess, we define a monotone decreasing sequence $\lambda_0^{(1)} > \lambda_1^{(1)} > \lambda_2^{(1)} > \dots > 0$ to explore progressively more liberal thresholds. Intuitively, if the anchor is too conservative ($r(\lambda_0^{(1)}) < \alpha$), relaxing the threshold can safely increase the yield. To guard against the possibility that the anchor itself may already be too liberal, we include a second decreasing path $\lambda_0^{(2)} > \lambda_1^{(2)} > \lambda_2^{(2)} > \dots \geq \lambda_0^{(1)}$ starting from a more conservative anchor, e.g., $\lambda_0^{(2)} = 1 - \alpha/2$.

For each candidate λ , we compute $UCB^{\text{pt}}(\lambda; \delta_*)$ for $r(\lambda)$ as described in Section 3.1, using $\delta_* = \delta/2$ since we consider $L = 2$ paths. In practice, we recommend using delta–method or bootstrap confidence bounds, resorting to finite–sample safeguards when the selected set is very small (e.g., ≤ 10). Along each path, the algorithm begins at the anchor and moves sequentially toward smaller λ . It stops when the upper confidence bound first exceeds the target level α , recording the last accepted value as $\hat{\lambda}_{\text{LTT}}^{(1)}$ or $\hat{\lambda}_{\text{LTT}}^{(2)}$, depending on the path. If no threshold is accepted, we set $\hat{\lambda}_{\text{LTT}}^{(l)} = 1$, corresponding to no selections. Finally, the calibrated LTT threshold is $\hat{\lambda}_{\text{LTT}} = \min\{\hat{\lambda}_{\text{LTT}}^{(1)}, \hat{\lambda}_{\text{LTT}}^{(2)}\}$. The complete procedure is summarized by Algorithm A4 in Appendix A1.4.

Compared to the greedy pointwise and uniform calibration methods from Sections 3.2–3.3, LTT offers a practical middle ground between efficiency and conservativeness. It typically enables the selection of larger patient subsets than uniform calibration while retaining a clear safety guarantee—something the greedy pointwise method lacks. A limitation of

LT is that it requires predefining the sequences of candidate thresholds, even though the most effective choice may depend on the data. The implementation described above, based on decreasing sequences starting from $\lambda_0^{(1)} = 1 - \alpha$ and $\lambda_0^{(2)} = 1 - \alpha/2$, performs well in many settings but may not be optimal in all cases. Another important consideration is the choice of the significance level δ , which governs a fundamental trade-off: smaller values (e.g., $\delta = 0.05$) yield stronger coverage guarantees but can reduce yield substantially, whereas larger values increase efficiency at the expense of interpretability and safety.

In the next section, we turn to a complementary framework based on conformal prediction and FDR control, which removes the need to specify a significance level δ .

4 Calibration via FDR Control with Conformal p -Values

4.1 Problem Statement and Connection to High-Probability Risk Control

The conformal prediction (Vovk et al., 2005) method adopts a hypothesis-testing rather than estimation-based perspective and aims to control the risk *in expectation* rather than with high-probability guarantees. Unlike the methods from Section 3, this approach calibrates a *cohort-level*, data-driven threshold $\hat{\lambda}$ for (1) that depends not only on the calibration data \mathcal{D}_{cal} but also on the covariates of the test cohort to which the screening rule is applied.

To formalize this setting, consider a test sample of m i.i.d. individuals from the target population, independent of both the models \hat{S} and \hat{G} and the calibration data \mathcal{D}_{cal} . Let

$$\mathcal{D}_{\text{test}} := \{(X_{n+j}, T_{n+j}, C_{n+j})\}_{j=1}^m,$$

denote the (unobserved) test data. In practice, only the covariates X_{n+1}, \dots, X_{n+m} are observed, and the goal is to identify a subset of low-risk test patients who are sufficiently unlikely to experience the event prior to a fixed time horizon t_0 . For each test individual $j \in [m]$, consider the hypothesis-testing problem

$$H_{n+j}^0 : T_{n+j} \leq t_0 \quad \text{vs.} \quad H_{n+j}^a : T_{n+j} > t_0, \quad (8)$$

where the null hypothesis H_{n+j}^0 states that patient j experiences the event before time t_0 . Note that these hypotheses are *random* because their truth status depends on the unobserved event times.

Our objective is to test these hypotheses simultaneously across all m test individuals while controlling the FDR. Following Jin and Candès (2023), we compute for each individual a *conformal p-value* $\hat{p}(X_{n+j})$, as detailed below, and reject H_{n+j}^0 whenever $\hat{p}(X_{n+j})$ is smaller than a suitable data-adaptive threshold $\hat{q}(\alpha) \in [0, 1]$. Formally, the selected set is

$$\hat{\mathcal{S}} = \{j \in [m] : \hat{p}(X_{n+j}) \leq \hat{q}(\alpha)\}, \quad (9)$$

where $\hat{q}(\alpha)$ depends on both \mathcal{D}_{cal} and $\mathcal{D}_{\text{test}}$, as detailed in the next section.

Let $\mathcal{H}_0 = \{j \in [m] : T_{n+j} \leq t_0\}$ denote the set of true null hypotheses. The false discovery proportion (FDP) is the fraction of selected patients who experience the event before t_0 , and the FDR is its expectation:

$$\text{FDP} = \frac{|\hat{\mathcal{S}} \cap \mathcal{H}_0|}{\max\{1, |\hat{\mathcal{S}}|\}}, \quad \text{FDR} = \mathbb{E}[\text{FDP}]. \quad (10)$$

The motivation for controlling the FDR is that this metric is closely related to the selected-set risk considered in Section 3, as formalized by the following result.

Proposition 1 *For $j \in [m]$, let $A(X_{n+j}) = \mathbb{I}[j \in \hat{\mathcal{S}}]$ denote the indicator of rejection for the hypothesis testing problem defined in (8), and let $r(A; \mathcal{D}_{\text{cal}})$ be the corresponding selection-set risk as defined in (2):*

$$r(A; \mathcal{D}_{\text{cal}}) = \mathbb{P}(T_{n+j} \leq t_0 \mid A(X_{n+j}) = 1, \mathcal{D}_{\text{cal}}).$$

Then,

$$\text{FDR} = \mathbb{E} \left[r(A; \mathcal{D}_{\text{cal}}) \cdot \mathbb{P}(|\hat{\mathcal{S}}| > 0 \mid \mathcal{D}_{\text{cal}}) \right].$$

Proposition 1 says that FDR control is approximately equivalent to controlling the selection-set risk *in expectation*, as long as selections are not too rare (i.e., $\mathbb{P}(|\hat{\mathcal{S}}| > 0 \mid \mathcal{D}_{\text{cal}}) \approx 1$). This connection makes the two frameworks comparable, and our empirical results will show that replacing high-probability risk control with FDR control can sometimes yield higher power. This result will also motivate extending FDR-controlling methods with the option to abstain depending on an empirical estimate of $\mathbb{P}(|\hat{\mathcal{S}}| > 0 \mid \mathcal{D}_{\text{cal}})$, as detailed below.

4.2 Computing Conformal p -Values

The hypotheses defined in (8) can be tested using conformal p -values constructed as follows. For each test individual $j \in [m]$, we compute a *nonconformity score* s_{n+j} based on the fitted survival model, measuring how plausible it is that this individual *survives beyond* time t_0 . Larger scores should indicate stronger evidence against $H_{n+j}^0 : T_{n+j} \leq t_0$. A simple and interpretable choice—though not the only possible one—is

$$s_{n+j} = \hat{S}(t_0 + \gamma \mid X_{n+j}),$$

where \hat{S} is the estimated survival function and $\gamma \geq 0$ is a user-specified offset parameter controlling how far beyond t_0 the survival probability is evaluated. The problem of optimally tuning γ , to maximize screening power, is discussed below.

To assess the relative magnitude of s_{n+j} in a distribution-free manner, we compare it to analogous scores computed on the calibration data, using the observed times instead of t_0 (Jin and Candès, 2023). Specifically, we define

$$s_i = \hat{S}(\tilde{T}_i + \gamma \mid X_i), \quad i \in [n], \quad s_{n+j} = \hat{S}(t_0 + \gamma \mid X_{n+j}), \quad j \in [m], \quad (11)$$

where $\tilde{T}_i = \min(T_i, C_i)$ denotes the observed time for the i -th individual.

The conformal p -value for test individual j is then given by

$$\hat{p}(X_{n+j}) = \frac{1 + \sum_{i=1}^n E_i \mathbb{I}\{\tilde{T}_i \leq t_0\} w_i \mathbb{I}\{s_i \geq s_{n+j}\}}{1 + n}, \quad (12)$$

where each calibration observation is weighted using the event-time IPCW approach:

$$w_i = \frac{1}{\hat{G}(\tilde{T}_i^- \mid X_i)}. \quad (13)$$

In words, $\hat{p}(X_{n+j})$ represents the (weighted) empirical rank of s_{n+j} among calibration scores corresponding to individuals who experienced the event before t_0 , adjusted via IPCW to account for censoring.

Sesia and Svetnik (2025b) show that, under conditionally independent censoring ($T \perp\!\!\!\perp C \mid X$), standard regularity conditions, and consistency of \hat{G} , the conformal p -values satisfy the approximate *marginal super-uniformity* property:

$$\mathbb{P}[\hat{p}(X_{n+j}) \leq \alpha, T_{n+j} \leq t_0] \leq \alpha, \quad \forall \alpha \in (0, 1).$$

Because the hypotheses are themselves random (data dependent), $\hat{p}(X_{n+j})$ is not a classical p -value, and it is not necessarily super-uniform *conditional* on H_{n+j}^0 being true—distinguishing this setup from other uses of conformal p -values (Bates et al., 2023). Nevertheless, small values of $\hat{p}(X_{n+j})$ provide evidence against the null, and marginal super-uniformity is sufficient to achieve asymptotically valid FDR control when applying the BH procedure (Benjamini and Hochberg, 1995) to $(\hat{p}(X_{n+1}), \dots, \hat{p}(X_{n+m}))$; i.e.,

$$\limsup_{n \rightarrow \infty} \text{FDR} \leq \alpha.$$

See Theorem 3 in Sesia and Svetnik (2025b) for a rigorous statement of this result.

A practical advantage of this method is that it requires neither a pre-specified threshold grid nor a confidence level δ . The user only needs to specify the target risk level α (for example, 10%) to obtain a calibrated selection rule. Its main limitation arises in the rare-selection regime, when $\mathbb{P}(R > 0)$ is small, as the FDR may then underestimate the conditional event rate among selected individuals. However, a simple stabilization correction can mitigate this issue: one can estimate $\mathbb{P}(R > 0 \mid \mathcal{D}_{\text{cal}})$ via a nonparametric bootstrap of the test-set p -values—resampling test individuals and reapplying the BH procedure—and then abstain if the estimated probability falls below a reasonable threshold (for instance, 0.9). This approach is described in the method outline provided by Algorithm 1.

Algorithm 1 Conformal screening with FDR control.

input Pre-trained survival model $\hat{S}(\cdot \mid x)$ and censoring model $\hat{G}(\cdot \mid x)$; right-censored calibration data $\mathcal{D}_{\text{cal}} = \{(X_i, \tilde{T}_i, E_i)\}_{i=1}^n$; test covariates $\{X_{n+1}, \dots, X_{n+m}\}$; target risk level $\alpha \in (0, 1)$; offset parameter $\gamma \geq 0$; selection stability threshold $\nu \in [0, 1]$.

- 1: For each $i \in [n]$, compute $w_i = E_i \mathbb{I}\{\tilde{T}_i \leq t_0\}/\hat{G}(\tilde{T}_i^- \mid X_i)$, with winsorization.
- 2: For each $i \in [n]$ and $j \in [m]$, compute s_i and s_{n+j} as in (11), with offset γ .
- 3: For each $j \in [m]$, compute a conformal p -value $\hat{p}(X_{n+j})$ as in (12).
- 4: Apply BH at level α to $\{\hat{p}(X_{n+j})\}_{j=1}^m$, and denote the rejection set as $\hat{\mathcal{S}} \subseteq [m]$.
- 5: (Optionally abstain) Compute an estimate $\hat{\mathbb{P}}(R > 0)$ of $\mathbb{P}(R > 0)$, where $R = |\hat{\mathcal{S}}|$, by nonparametric bootstrap over test rows; set $\hat{\mathcal{S}} = \emptyset$ if $\hat{\mathbb{P}}(R > 0) < \nu$.

output Selected subset of patients $\hat{\mathcal{S}} \subseteq [m]$.

The parameter γ appearing in the computation of the nonconformity scores through $r = \hat{S}(\cdot + \gamma \mid x)$ plays an important role in maximizing selection power, and we have empirically observed that its optimal choice is typically data-dependent. For this reason, we recommend tuning γ using a cross-validation scheme applied to an independent data

set drawn from the same distribution but disjoint from the calibration data, as to maintain the exchangeability with the test data required for valid FDR control. For example, one can re-use for this purpose the same training data employed for fitting the survival and censoring models, as detailed by Algorithm A5 in Appendix A2.

Finally, it is worth emphasizing that this method is inherently transductive, or *cohort-adaptive*: it selects a subset of test patients without defining an inductive screening rule. For interpretability, however, since the conformal p -values are monotone in the risk score $\hat{s}(x)$, one can report the implied cohort threshold

$$\tilde{\lambda} := \inf \{ \hat{s}(X_{n+j}) : \hat{p}(X_{n+j}) \leq \alpha R/m \},$$

corresponding to the smallest score among the selected patients, where R denotes the number selected and m the cohort size. This threshold summarizes the calibrated screening rule for the current batch but is not technically valid for a different cohort.

5 Numerical Experiments with Semi-Synthetic Data

We conduct empirical comparisons of different calibration methods using semi-synthetic data designed to approximately replicate the structure of a real oncology data set while providing full knowledge of the true event times for all patients. First, using the observed data, we fit models for both the event-time and censoring-time distributions conditional on the covariates, employing standard survival modeling approaches. These “generative” models are used to simulate synthetic survival and censoring times conditional on the original covariates. This setup enables full evaluation of method performance, while attempting to preserve the multivariate structure and clinical realism of the original cohort.

5.1 Data Description

We examine data from the Flatiron Health Research Database (FHRD), an electronic health record-derived database comprising data from over 280 oncology practices at 800+ unique sites of care in the US, spanning the period from December 2010 to May 2023 (Ma et al., 2020; Birnbaum et al., 2020; Becker et al., 2020; Johnson et al., 2025). All data are de-identified and subject to technical and administrative safeguards to protect patient confidentiality.

We focus on a cohort of 7,000 patients diagnosed with advanced non-small cell lung cancer (aNSCLC). For each patient, 43 covariates describe demographic and socioeconomic characteristics, smoking status, vital signs, functional status, comorbidity index, tumor histology, number and location of metastatic sites, treatment history, indicators of prior laboratory assessments, and a wide range of clinical laboratory measurements. The outcome measures include a binary event indicator and the corresponding time to event or censoring.

5.2 Semi-Synthetic Data Generation

Let $X = \{X_i\}_{i=1}^{N_0}$ denote the covariate matrix from the FHRD, with $N_0 = 7,000$ rows and 43 columns. These covariates are treated as fixed design points representing the target population. Using all available observations to approximate this population as closely as possible, we fit two separate *generative* models, respectively denoted as (\hat{S}^*, \hat{G}^*) , to estimate

the conditional distribution of the survival and censoring times given the covariates. We use standard modeling approaches for this task: a Cox proportional hazards model (Cox, 1972), and a generalized random forest (GRF) survival model implemented in the `grf` R package. The censoring model \hat{G}^* is fit similar to \hat{S}^* after flipping the event indicators.

For each pair of generative models and each individual i , we generate independent uniform random variables $U_i, V_i \sim \text{Uniform}(0, 1)$ and define event and censoring times as

$$T_i = \inf\{t : \hat{S}^*(t | X_i) \leq U_i\}, \quad C_i = \inf\{t : \hat{G}^*(t | X_i) \leq V_i\},$$

which guarantees conditionally independent censoring by construction. The observed semi-synthetic data for the i -th individual are then given by (X_i, \tilde{T}_i, E_i) , where $\tilde{T}_i = \min(T_i, C_i)$ and $E_i = \mathbb{I}\{T_i < C_i\}$. This process produces a new right-censored dataset with realistic dependence patterns and known ground-truth event times. The full resampling procedure is independently repeated $R = 100$ times.

5.3 Analysis Protocol

For each replicate of the semi-synthetic data, the observations are randomly split into a training set of size $n_{\text{tr}} = 5,000$, a calibration set of size $n_{\text{cal}} = 1,000$, and a test set of size $n_{\text{te}} = 1,000$. We consider four screening horizons, $t_0 \in \{2, 3, 6, 9\}$ months, and aim to select a low-risk subgroup with a target event-rate of $\alpha = 0.10$, corresponding to survival probability approximately 0.90 by time t_0 . The training data are used to fit survival and censoring models, using one of three approaches: the first two are the Cox proportional hazards model and generalized random forest also used as generative models, and the third approach is an accelerated failure time gradient boosting model implemented in the `xgboost` R package. This setup allows studying robustness of different methods under both correctly specified and misspecified settings. In each case, the calibration data are used to calibrate the screening rule, and the test data to evaluate performance.

We compare four calibration methods and two benchmarks, all relying on the same fitted survival and censoring models. The first method is *greedy pointwise calibration* (Section 3.2), which selects the largest feasible threshold based on pointwise upper confidence bounds. The second is the *uniform calibration* approach (Section 3.3), implemented using Gaussian-multiplier perturbations with 1000 Gaussian draws to construct simultaneous confidence bounds. The third method is *learn-then-test (LT)* calibration (Section 3.4). These three methods share a threshold grid defined by 200 quantiles of the calibration score distribution and use pointwise risk estimates based on asymptotic delta-method approximations, reverting to empirical Bernstein finite-sample bounds whenever the number of selected patients is below 10. By default, these three methods are applied at significance level $\delta = 0.10$, although we also explore the effect of using different values of δ . The fourth method is the *conformal* approach from Section 4, for which we tune the offset parameter γ using the training data according to the procedure described in Appendix A2. To ensure consistency with the other calibration methods, as suggested by Proposition 1, the conformal approach abstains whenever a bootstrap estimate of $\mathbb{P}(R > 0)$ falls below 0.9.

For comparison, we also include two additional benchmarks: a *model-based* baseline, which treats the predicted survival probabilities as if they were exact and selects the largest subset of test patients with average predicted survival above 0.90, using both training and

calibration data for model fitting; and an ideal *oracle* that uses the true generative survival function $S^*(t | x)$ to select the largest subset with 90% average survival, representing the best achievable performance under perfect knowledge of the data-generating process.

Unless specified otherwise, all IPCW-based methods use the same event-time weights, to simplify the comparison. To mitigate instability from extreme censoring, the IPCW weights are winsorized at the 99th percentile within the calibration split.

5.4 Evaluation Metrics

For each replicate and time horizon t_0 , we record the following performance measures. The first is *yield*: the number of test patients selected by the calibrated rule. The second is the *selected-set survival rate*, defined as the proportion of selected individuals who do not experience the event by time t_0 , with the convention that if no individuals are selected then the survival rate is counted as being one. We also report the selected-set survival rate *conditionally* on having selected at least one patient. Finally, we record whether at least one selection is made in a given replicate. The empirical distribution of all these metrics is summarized across the 100 replicates.

5.5 Results

Figure 1 summarizes the results for a well-specified setting, where both the data-generating and fitted models are generalized random forests. All methods successfully achieve the target survival rate across all time horizons but differ in yield. The conformal approach selects the most patients, typically followed by the greedy and LTT high-probability procedures, while the uniform method is overly conservative. At longer screening horizons, the number of selected patients naturally declines for all methods. Moreover, the conditional survival among selected patients occasionally falls slightly below the target level; this behavior reflects the limitations of asymptotic approximations, on which all these methods rely, when the effective sample size is very small. Robustness to small sample sizes could be improved by applying the finite-sample fallback more aggressively—for example, when fewer than 20–30 patients are selected instead of only below 10—at the expense of reduced yield. A detailed numerical summary of these results is reported in Table A1 in Appendix A3.1.

Figure 2 illustrates how the choice of significance level δ affects the behavior of the LTT method, in the same setting as Figure 1. More conservative significance levels (e.g., $\delta = 0.05$) lead to low-yield screening rules, substantially yield. In contrast, when applied with very liberal significance levels (e.g., $\delta = 0.5$), LTT leads to screening rules behaving more similar to those obtained with the conformal approach. The interpretation, however, differs. The conformal method ensures that the event rate among selected patients does not exceed 10% on average, providing an expectation-level guarantee. LTT with $\delta = 0.5$, on the other hand, guarantees only that the event rate will fall below 10% in at least half of repeated experiments (i.e., with probability 0.5), offering no control over how large the event rate might be in the remaining 50% of cases. Because the event rate is bounded below by 0% but can substantially exceed the 10% target, controlling its *expected value* is more meaningful than controlling it in probability at a very low confidence level such as 50%.

Figure 3 presents results from experiments analogous to those in Figure 1, except that the survival model is now misspecified: a gradient boosting model is fitted on data generated

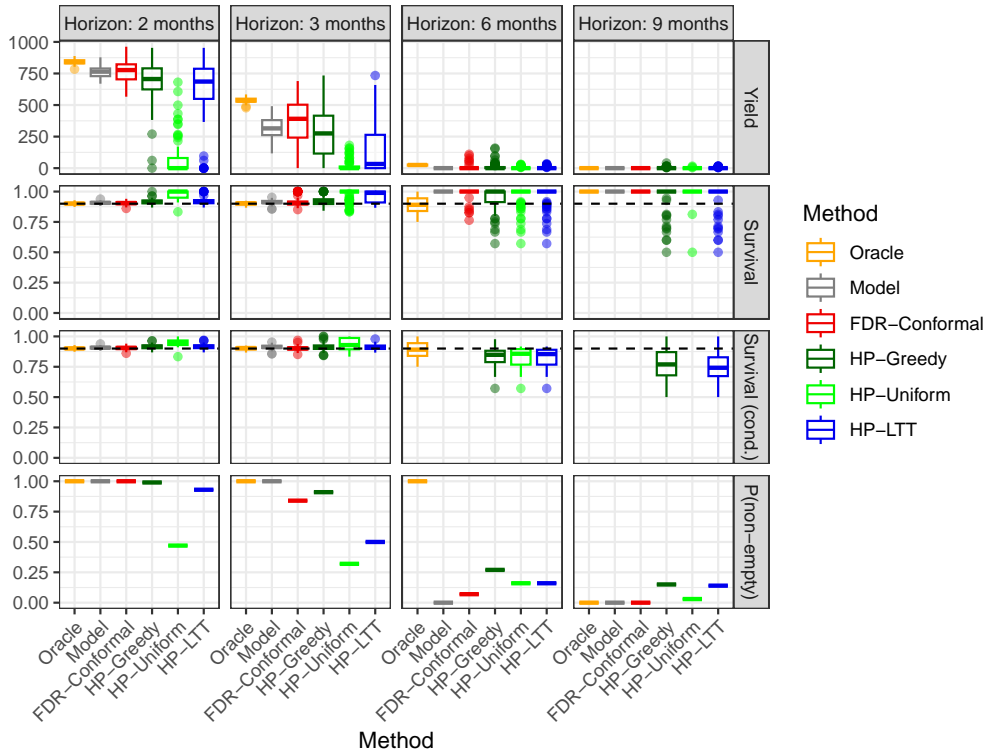


Figure 1: Summary of low-risk screening results obtained with different calibration methods on semi-synthetic data, at different screening horizons. Top row: yield. Second row: survival rate among selected patients. Third row: survival rate among selected patients, conditional on at least one patient being selected. Conditional results are not evaluated if selections occur in fewer than 10% of experiments. The dashed horizontal lines denotes the target survival rate (e.g., 90%). Fourth row: proportion of experiments in which at least one patient is selected. All methods use the same survival and censoring models based on random forests. High-probability (HP) methods are applied at confidence level $\delta = 0.1$.

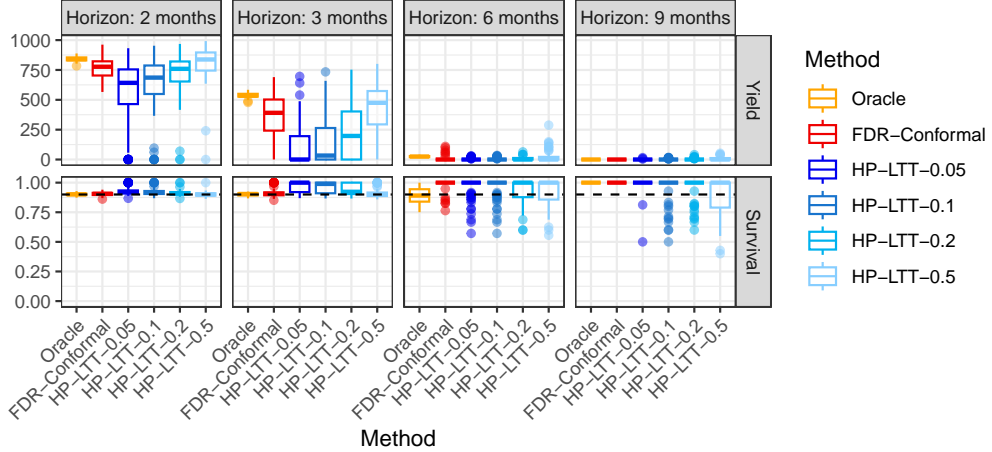


Figure 2: Summary of low-risk screening results on semi-synthetic data, as in Figure 1. Here, the LTT calibration method is applied at different confidence levels δ , ranging from $\delta = 0.05$ (more conservative) to $\delta = 0.5$ (more liberal).

from a random forest-based generative model. As before, the high-probability calibration methods use a significance level of $\delta = 0.1$. In this setting, the uncalibrated model selects too many patients and fails to achieve the target survival rate at longer horizons. By contrast, all calibrated methods successfully control the event rate below the 10% target, though their yields decline markedly as the time horizon t_0 increases. The relative performance ordering among valid calibration methods remains consistent with the well-specified case, with the conformal approach selecting the most patients on average. A detailed numerical summary is provided in Table A2 in Appendix A3.1. Figure A1 and Table A3 summarize qualitatively similar results obtained using the Cox model instead of gradient boosting.

Figure 4 illustrates how the screening yield of all calibration methods tends to increase with the number of calibration samples. These results correspond to numerical experiments similar to those in Figure 1, using a fixed screening horizon of $t_0 = 2$ months and comparing all three fitted survival models considered so far: the Cox model, the generalized random forest (GRF), and gradient boosting (XGB). In this setting, the conformal approach performs quite similarly to the ideal oracle when the calibration sample size is large enough, while LTT suffers the steepest performance decline when calibration data are scarce. Additional results following the same layout of Figure 1 but using a smaller calibration sample size ($n_{\text{cal}} = 100$) are provided in Figures A2–A3 and Table A4 in Appendix A3.1. These results highlight that variability increases and the number of selected patients decreases as n_{cal} becomes small. Despite this loss in precision, all procedures maintain the target survival rate on average. The uniform approach remains the most conservative calibration method, while conformal calibration consistently achieves the highest yield among valid approaches, provided that selections are not exceedingly rare.

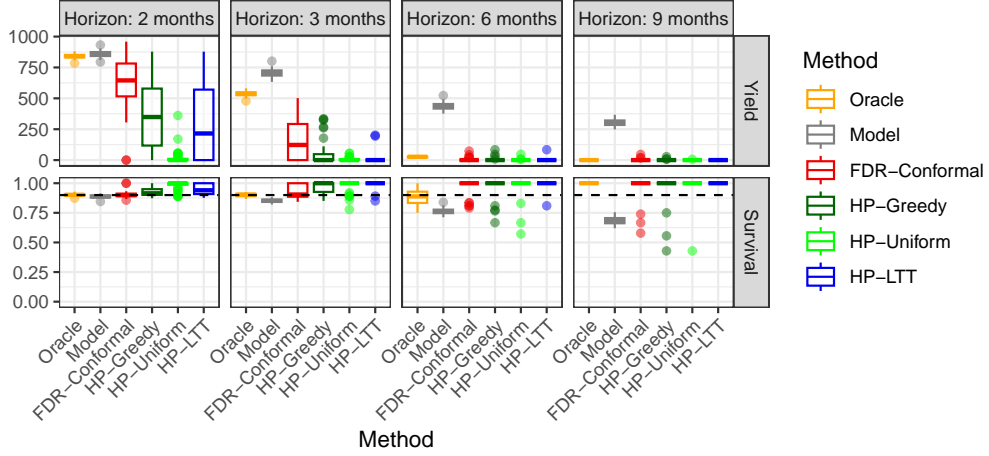


Figure 3: Summary of low-risk screening results obtained by applying different calibration methods to semi-synthetic data simulated using a random forest generative model, at different screening horizons. All methods use the same mis-specified gradient boosting survival model, which leads to lower-than-expected survival rates at long horizons if applied to select low-risk patients without calibration. Other details as in Figure 1.

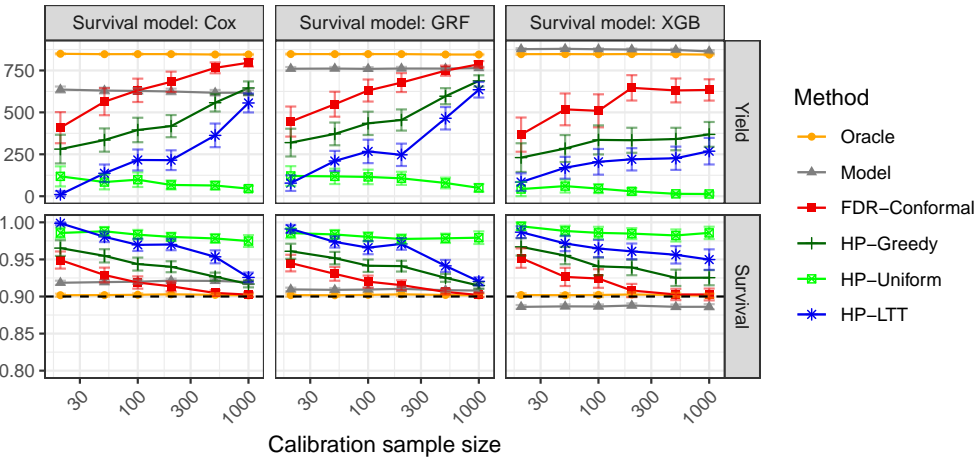


Figure 4: Average performance of low-risk screening methods on semi-synthetic data, as in Figure 1, at horizon $t_0 = 2$ months. The results are shown as a function of the calibration sample size, for different survival models. Error bars represent two standard errors.

6 Application to FHRD data

We next apply the described calibration methods directly to the FHRD data described in Section 5.1, using the true observed times and censoring indicators. We randomly divide the 7,000 observations into a training set of 5,000, a calibration set of 1,000, and a test set of 1,000, and we average all reported results over 100 independent splits. Because the event times are only partially observed, we report IPCW-adjusted point estimates of survival rates together with surrogate upper and lower bounds obtained by treating censored observations optimistically or pessimistically, respectively. Aside from this adjustment, we follow the same analysis protocol used for the semi-synthetic experiments in Section 5.3. In particular, we use a generalized random forest model to estimate the censoring distribution and evaluate three survival models (i.e., gradient boosting, the Cox model, and a generalized random forest) for estimating the event-time distribution.

Table 1 summarizes the results when gradient boosting is used to model the survival distribution, with a visual summary provided in Figure A4 in Appendix A3.2. Overall, these findings closely mirror those from the semi-synthetic experiments. Across all time horizons, the conformal method and all high-probability calibration procedures achieve selected-set survival rates near the target level on average, including the greedy pointwise approach. The conformal method consistently selects the most patients, typically outperforming both the greedy and LTT approaches, while the uniform calibration method remains overly conservative. As the prediction horizon increases, selections become rarer and variability increases across all methods. In sharp contrast to the calibrated procedures, the uncalibrated model benchmark selects far too many patients and yields survival rates well below the desired 90% level, particularly at longer time horizons.

Tables A5–A6 and Figures A5–A6 in Appendix A3.2 show analogous results for the Cox model and the generalized random forest. The overall trends closely match those in Table 1 and Figure A4: the calibrated methods achieve survival rates near the target level on average, with the conformal approach typically yielding the largest selections and the uniform method remaining conservative. In these two settings, however, the uncalibrated model leads to a conservative rather than overly liberal screening rule. Finally, Figures A7–A9 in Appendix A3.2 visualize the effect of changing the significance level δ used by the LTT approach, with results analogous to those reported in Figure 2.

Table 1: Summary of low-risk screening results on FHRD data across different screening horizons. Because of censoring, survival rates cannot be evaluated exactly; instead, we report deterministic lower (LB) and upper (UB) bounds for both the marginal survival rate (Surv.) and the conditional survival rate given at least one selection (C.Surv.). We also report the fraction of trials with at least one selected patient, $P(|S| > 0)$. Each entry shows the mean and, in parentheses, two standard errors across repeated splits. Values highlighted in red indicate survival rates significantly below the 90% target, while boldface denotes the method achieving the largest number of selections among those with valid survival rates.

Method	Yield	Surv.(LB)	Surv.(UB)	C.Surv.(LB)	C.Surv.(UB)	$P(S > 0)$
Horizon: 2 months						
Model	836 (4.06)	0.88 (0.00)	0.91 (0.00)	0.88 (0.00)	0.91 (0.00)	1.00 (0.00)
FDR-Conformal	883 (15.35)	0.88 (0.00)	0.90 (0.00)	0.88 (0.00)	0.90 (0.00)	1.00 (0.00)
HP-Greedy	790 (23.29)	0.89 (0.00)	0.92 (0.00)	0.89 (0.00)	0.92 (0.00)	1.00 (0.00)
HP-Uniform	133 (58.13)	0.96 (0.01)	0.98 (0.01)	0.94 (0.01)	0.97 (0.01)	0.63 (0.15)
HP-LTT	783 (26.91)	0.89 (0.00)	0.92 (0.00)	0.89 (0.00)	0.92 (0.00)	1.00 (0.00)
Horizon: 3 months						
Model	714 (4.73)	0.85 (0.00)	0.89 (0.00)	0.85 (0.00)	0.89 (0.00)	1.00 (0.00)
FDR-Conformal	590 (28.11)	0.86 (0.01)	0.90 (0.01)	0.86 (0.01)	0.90 (0.01)	1.00 (0.00)
HP-Greedy	466 (32.85)	0.88 (0.01)	0.92 (0.01)	0.88 (0.01)	0.92 (0.01)	1.00 (0.00)
HP-Uniform	30 (18.38)	0.97 (0.02)	0.99 (0.01)	0.92 (0.01)	0.97 (0.01)	0.43 (0.15)
HP-LTT	375 (54.75)	0.90 (0.01)	0.93 (0.01)	0.88 (0.01)	0.92 (0.01)	0.86 (0.11)
Horizon: 6 months						
Model	505 (5.24)	0.76 (0.00)	0.83 (0.00)	0.76 (0.00)	0.83 (0.00)	1.00 (0.00)
FDR-Conformal	139 (24.65)	0.84 (0.02)	0.92 (0.01)	0.82 (0.01)	0.91 (0.01)	0.90 (0.09)
HP-Greedy	43 (18.10)	0.92 (0.03)	0.96 (0.01)	0.84 (0.01)	0.93 (0.01)	0.49 (0.16)
HP-Uniform	4 (3.57)	0.98 (0.02)	0.99 (0.01)	0.88 (0.03)	0.96 (0.01)	0.15 (0.11)
HP-LTT	14 (13.97)	0.98 (0.02)	0.99 (0.01)	0.81 (0.01)	0.90 (0.01)	0.10 (0.09)
Horizon: 9 months						
Model	396 (5.69)	0.67 (0.01)	0.78 (0.01)	0.67 (0.01)	0.78 (0.01)	1.00 (0.00)
FDR-Conformal	17 (10.20)	0.92 (0.04)	0.96 (0.02)	0.75 (0.03)	0.88 (0.02)	0.33 (0.16)
HP-Greedy	4 (4.25)	0.96 (0.03)	0.98 (0.02)	0.72 (0.03)	0.87 (0.02)	0.14 (0.12)
HP-Uniform	0 (0.61)	0.99 (0.01)	0.99 (0.01)	NA	NA	0.03 (0.06)
HP-LTT	0 (0.00)	1.00 (0.00)	1.00 (0.00)	NA	NA	0.00 (0.00)

7 Discussion

The methods discussed in this paper extend naturally to more complex settings. Firstly, they can be applied symmetrically to calibrate high-risk screening rules, by simply inverting the score inequality (Sesia and Svetnik, 2025b). Moreover, they can be adapted to handle deviations from i.i.d. sampling, such as covariate shift, via additional reweighting (Tibshirani et al., 2019; Park et al., 2024; Jin and Candès, 2025). In the future, it would be interesting to extend the conformal approach by integrating it with recent developments in FDR control via e-values instead of p-values (Wang and Ramdas, 2022; Vovk and Wang, 2023; Lee and Ren, 2024), a direction that could for example lead to lower algorithmic variability due to random sample splitting (Bashari et al., 2023) and the possibility of incorporating additional constraints into the patient subset selection problem (Nair et al., 2025).

Acknowledgements

The authors thank Dr. Peining Tao and Dr. Michael Johnson for preparing the analytical dataset used in this study, and Dr. Mehmet Burcu for suggesting the problem of predicting short-term survival of oncology patients.

Software Availability

Software implementing the methods and experiments described in this paper is available at https://github.com/msesia/screening_calibration, along with usage examples.

References

Anastasios Angelopoulos, Stephen Bates, Adam Fisch, Lihua Lei, and Tal Schuster. Conformal risk control. In *International Conference on Learning Representations*, volume 2024, pages 55198–55218, 2024a.

Anastasios N Angelopoulos and Stephen Bates. Conformal prediction: A gentle introduction. *Foundations and trends® in machine learning*, 16(4):494–591, 2023.

Anastasios N Angelopoulos, Rina Foygel Barber, and Stephen Bates. Theoretical foundations of conformal prediction. *arXiv preprint arXiv:2411.11824*, 2024b.

Anastasios N Angelopoulos, Stephen Bates, Emmanuel Candès, Michael I Jordan, and Lihua Lei. Learn then test: Calibrating predictive algorithms to achieve risk control. *Ann. Appl. Stat.*, 19(2):1641–1662, 2025.

Avinash Barnwal, Hyunsu Cho, and Toby Hocking. Survival regression with accelerated failure time model in xgboost. *J. Comput. Graph. Stat.*, 31(4):1292–1302, 2022.

Meshi Bashari, Amir Epstein, Yaniv Romano, and Matteo Sesia. Derandomized novelty detection with fdr control via conformal e-values. In *Advances in Neural Information Processing Systems*, volume 36, pages 65585–65596, 2023.

Stephen Bates, Emmanuel Candès, Lihua Lei, Yaniv Romano, and Matteo Sesia. Testing for outliers with conformal p-values. *Ann. Stat.*, 51(1):149–178, 2023.

Peter Bauer. Multiple testing in clinical trials. *Stat. Med.*, 10(6):871–890, 1991.

T Becker, J Weerpals, AM Jegg, WV So, A Fischer, M Weisser, F Schmich, D Rüttinger, and A Bauer-Mehren. An enhanced prognostic score for overall survival of patients with cancer derived from a large real-world cohort. *Ann. Oncol.*, 31(11):1561–1568, 2020.

Yoav Benjamini and Yosef Hochberg. Controlling the false discovery rate: a practical and powerful approach to multiple testing. *J. R. Stat. Soc. Ser. B Methodol.*, 57(1):289–300, 1995.

Savannah Bergquist, Gabriel A Brooks, Mary Beth Landrum, Nancy L Keating, and Sherri Rose. Uncertainty in lung cancer stage for survival estimation via set-valued classification. *Stat. Med.*, 41(19):3772–3788, 2022.

Dimitris Bertsimas and Holly Wiberg. Machine learning in oncology: methods, applications, and challenges. *JCO Clin. Cancer Inform.*, 4:CCI–20, 2020.

Kassu Mehari Beyene, Ding-Geng Chen, and Yehenew Getachew Kifle. A novel nonparametric time-dependent precision–recall curve estimator for right-censored survival data. *Biometrical Journal*, 66(3):2300135, 2024.

Benjamin Birnbaum, Nathan Nussbaum, Katharina Seidl-Rathkopf, Monica Agrawal, Melissa Estevez, Evan Estola, Joshua Haimson, Lucy He, Peter Larson, and Paul Richardson. Model-assisted cohort selection with bias analysis for generating large-scale cohorts from the EHR for oncology research. *arXiv preprint arXiv:2001.09765*, 2020.

P Blanche and MP Blanche. Package ‘timeroc’: time-dependent ROC curve and AUC for censored survival data. *Vienna: R Foundation for Statistical Computing*, 2013.

Emmanuel Candès, Lihua Lei, and Zhimei Ren. Conformalized survival analysis. *J. R. Stat. Soc. Ser. B Methodol.*, 85(1):24–45, 2023.

Stephen R Cole and Miguel A Hernán. Constructing inverse probability weights for marginal structural models. *Am. J. Epidemiol.*, 168(6):656–664, 2008.

David R Cox. Regression models and life-tables. *J. R. Stat. Soc. Ser. B Methodol.*, 34(2): 187–202, 1972.

Hen Davidov, Shai Feldman, Gil Shamai, Ron Kimmel, and Yaniv Romano. Conformalized survival analysis for general right-censored data. In *International Conference on Learning Representations*, 2025.

Rebecca Farina, Eric J Tchetgen Tchetgen, and Arun Kumar Kuchibhotla. Doubly robust and efficient calibration of prediction sets for censored time-to-event outcomes. *arXiv preprint arXiv:2501.04615*, 2025.

Thomas R Fleming and David P Harrington. *Counting processes and survival analysis*. John Wiley & Sons, 2013.

Yu Gui, Rohan Hore, Zhimei Ren, and Rina Foygel Barber. Conformalized survival analysis with adaptive cut-offs. *Biometrika*, 111(2):459–477, 2024.

Patrick J Heagerty and Yingye Zheng. Survival model predictive accuracy and ROC curves. *Biometrics*, 61(1):92–105, 2005.

Patrick J Heagerty, Thomas Lumley, and Margaret S Pepe. Time-dependent ROC curves for censored survival data and a diagnostic marker. *Biometrics*, 56(2):337–344, 2000.

Hemant Ishwaran, Udaya B. Kogalur, Eugene H. Blackstone, and Michael S. Lauer. Random survival forests. *Ann. Appl. Stat.*, 2(3):841 – 860, 2008.

Ying Jin and Emmanuel Candès. Selection by prediction with conformal p-values. *J. Mach. Learn. Res.*, 24(244):1–41, 2023.

Ying Jin and Emmanuel Candès. Model-free selective inference under covariate shift via weighted conformal p-values. *Biometrika*, page asaf066, 2025.

Michael Johnson, Peining Tao, Mehmet Burcu, John Kang, Richard Baumgartner, Junshui Ma, and Vladimir Svetnik. Creating a proxy for baseline eastern cooperative oncology group performance status in electronic health records for comparative effectiveness research in advanced non-small cell lung cancer. *JCO Clin. Cancer Inform.*, 9:e2400185, 2025.

Jared L Katzman, Uri Shaham, Alexander Cloninger, Jonathan Bates, Tingting Jiang, and Yuval Kluger. DeepSurv: personalized treatment recommender system using a Cox proportional hazards deep neural network. *BMC Med. Res. Methodol.*, 18:1–12, 2018.

Junu Lee and Zhimei Ren. Boosting e-BH via conditional calibration. *arXiv preprint arXiv:2404.17562*, 2024.

Jing Lei, Max G’Sell, Alessandro Rinaldo, Ryan J Tibshirani, and Larry Wasserman. Distribution-free predictive inference for regression. *J. Am. Stat. Assoc.*, 113(523):1094–1111, 2018.

Xinran Ma, Lura Long, Sharon Moon, Blythe JS Adamson, and Shrujal S Baxi. Comparison of population characteristics in real-world clinical oncology databases in the US: Flatiron Health, SEER, and NPCR. *Medrxiv*, pages 2020–03, 2020.

Andreas Maurer and Massimiliano Pontil. Empirical bernstein bounds and sample variance penalization. *arXiv preprint arXiv:0907.3740*, 2009.

Yash Nair, Ying Jin, James Yang, and Emmanuel Candès. Diversifying conformal selections. *arXiv preprint arXiv:2506.16229*, 2025.

Henrik Olsson, Kimmo Kartasalo, Nita Mulliqi, Marco Capuccini, Pekka Ruusuvuori, Hemamali Samaratunga, Brett Delahunt, Cecilia Lindskog, Emiel AM Janssen, Anders Blilie, et al. Estimating diagnostic uncertainty in artificial intelligence assisted pathology using conformal prediction. *Nat. Comm.*, 13(1):7761, 2022.

Sangdon Park, Edgar Dobriban, Insup Lee, and Osbert Bastani. PAC prediction sets under covariate shift. In *International Conference on Learning Representations*, volume 2024, 2024.

Yuhyun Park and LJ Wei. Estimating subject-specific survival functions under the accelerated failure time model. *Biometrika*, 90(3):717–723, 2003.

Jing Qin, Jin Piao, Jing Ning, and Yu Shen. Conformal predictive intervals in survival analysis: a resampling approach. *Biometrics*, 81(2):ujaf063, 2025.

James M Robins. Information recovery and bias adjustment in proportional hazards regression analysis of randomized trials using surrogate markers. In *Proc. Biopharm. Sect. Am. Stat. Assoc.*, volume 24, pages 24–33. San Francisco CA, 1993.

James M Robins and Andrea Rotnitzky. Recovery of information and adjustment for dependent censoring using surrogate markers. In *AIDS epidemiology: methodological issues*, pages 297–331. Springer, 1992.

Matteo Sesia and Vladimir Svetnik. Doubly robust conformalized survival analysis with right-censored data. In *International Conference on Machine Learning*. PMLR, 2025a.

Matteo Sesia and Vladimir Svetnik. Conformal survival bands for risk screening under right-censoring. In *Proceedings of the Fourteenth Symposium on Conformal and Probabilistic Prediction with Applications*, volume 266 of *Proceedings of Machine Learning Research*, pages 464–514. PMLR, 10–12 Sep 2025b.

Ryan J Tibshirani, Rina Foygel Barber, Emmanuel Candès, and Aaditya Ramdas. Conformal prediction under covariate shift. *Advances in neural information processing systems*, 32, 2019.

Hajime Uno, Tianxi Cai, Lu Tian, and Lee-Jen Wei. Evaluating prediction rules for t-year survivors with censored regression models. *J. Am. Stat. Assoc.*, 102(478):527–537, 2007.

Janette Vazquez and Julio C Facelli. Conformal prediction in clinical medical sciences. *J. Healthc. Inform. Res.*, 6(3):241–252, 2022.

David M Vock, Julian Wolfson, Sunayan Bandyopadhyay, Gediminas Adomavicius, Paul E Johnson, Gabriela Vazquez-Benitez, and Patrick J O’Connor. Adapting machine learning techniques to censored time-to-event health record data: A general-purpose approach using inverse probability of censoring weighting. *J. Biomed. Inform.*, 61:119–131, 2016.

Vladimir Vovk and Ruodu Wang. Confidence and discoveries with e-values. *Statistical Science*, 38(2):329–354, 2023.

Vladimir Vovk, Alexander Gammerman, and Glenn Shafer. *Algorithmic learning in a random world*, volume 29. Springer, 2005.

Ruodu Wang and Aaditya Ramdas. False discovery rate control with e-values. *J. R. Stat. Soc. Ser. B Methodol.*, 84(3):822–852, 2022.

Yan Yuan, Qian M Zhou, Bingying Li, Hengrui Cai, Eric J Chow, and Gregory T Armstrong. A threshold-free summary index of prediction accuracy for censored time to event data. *Stat. Med.*, 37(10):1671–1681, 2018.

Yingye Zheng, Tianxi Cai, Margaret S Pepe, and Wayne C Levy. Time-dependent predictive values of prognostic biomarkers with failure time outcome. *J. Am. Stat. Assoc.*, 103(481):362–368, 2008.

Yingye Zheng, Tianxi Cai, Janet L Stanford, and Ziding Feng. Semiparametric models of time-dependent predictive values of prognostic biomarkers. *Biometrics*, 66(1):50–60, 2010.

Appendix A1. Calibration via High-Probability Risk Control

A1.1 Pointwise Risk Estimation

For a fixed threshold λ , recall that the population-level *selected-set risk* is defined as

$$r(\lambda) = \frac{\theta(\lambda)}{\mu(\lambda)}, \quad \theta(\lambda) = \mathbb{E}[\mathbb{I}\{T \leq t_0\} A_\lambda(X)], \quad \mu(\lambda) = \mathbb{E}[A_\lambda(X)],$$

where $A_\lambda(X)$ indicates whether a patient with covariates X would be selected by the screening rule at threshold λ . Using the calibration data, we estimate these quantities as

$$\hat{r}(\lambda) = \frac{\hat{\theta}(\lambda)}{\hat{\mu}(\lambda)},$$

where $\hat{\theta}$ and $\hat{\mu}$ are obtained with either IPCW-ET (5) or IPCW-FT (6).

A1.1.1 ASYMPTOTIC BOUNDS VIA DELTA METHOD

We review here how to construct an approximate $(1 - \delta)$ upper confidence bound for the true risk $r(\lambda)$ using the delta method.

Define the function $g(\theta, \mu) = \theta/\mu$, so that $\hat{r}(\lambda) = g(\hat{\theta}, \hat{\mu})$. The gradient of g is

$$\nabla g(\theta, \mu) = \begin{pmatrix} 1/\mu \\ -\theta/\mu^2 \end{pmatrix}.$$

By the multivariate delta method, the asymptotic variance of $\hat{r}(\lambda)$ is approximated by

$$\hat{\sigma}^2(\lambda) = \nabla g(\hat{v})^\top \hat{\Sigma}(\lambda) \nabla g(\hat{v}),$$

where $\hat{v} = (\hat{\theta}, \hat{\mu})^\top$ and

$$\hat{\Sigma}(\lambda) = \begin{pmatrix} \hat{\Sigma}_{\theta\theta}(\lambda) & \hat{\Sigma}_{\theta\mu}(\lambda) \\ \hat{\Sigma}_{\mu\theta}(\lambda) & \hat{\Sigma}_{\mu\mu}(\lambda) \end{pmatrix}$$

denotes the empirical covariance matrix of $(\hat{\theta}(\lambda), \hat{\mu}(\lambda))$. Each block in $\hat{\Sigma}(\lambda)$ is estimated from individual sample contributions:

$$\hat{\Sigma}_{ab}(\lambda) = \frac{1}{n} \sum_{i=1}^n (\psi_i^{(a)}(\lambda) - \bar{\psi}^{(a)}(\lambda)) (\psi_i^{(b)}(\lambda) - \bar{\psi}^{(b)}(\lambda)), \quad a, b \in \{\theta, \mu\}.$$

The terms $\psi_i^{(\theta)}$ and $\psi_i^{(\mu)}$ represent each subject's contribution to the estimators of θ and μ , centered by their sample means. When using event-time weighting, these take the form:

$$\psi_i^{(\theta)} = A_\lambda(X_i) \frac{\mathbb{I}(\tilde{T}_i \leq t_0, E_i = 1)}{\hat{G}(\tilde{T}_i^- \mid X_i)} - \hat{\theta}_{\text{et}}(\lambda), \quad \psi_i^{(\mu)} = A_\lambda(X_i) - \hat{\mu}(\lambda).$$

Alternatively, under fixed-time weighting:

$$\psi_i^{(\theta)} = A_\lambda(X_i) \left(1 - \frac{\mathbb{I}(\tilde{T}_i \geq t_0)}{\hat{G}(t_0 \mid X_i)} \right) - \hat{\theta}_{\text{ft}}(\lambda), \quad \psi_i^{(\mu)} = A_\lambda(X_i) - \hat{\mu}(\lambda).$$

Expanding the expression for the asymptotic variance of $\hat{r}(\lambda)$ gives:

$$\hat{\sigma}^2(\lambda) = \frac{\hat{\Sigma}_{\theta\theta}(\lambda)}{\hat{\mu}^2(\lambda)} - 2 \frac{\hat{\theta}(\lambda)}{\hat{\mu}^3(\lambda)} \hat{\Sigma}_{\theta\mu}(\lambda) + \frac{\hat{\theta}^2(\lambda)}{\hat{\mu}^4(\lambda)} \hat{\Sigma}_{\mu\mu}(\lambda).$$

Equivalently, this can be written as a single sample variance:

$$\hat{\sigma}^2(\lambda) = \frac{1}{n} \sum_{i=1}^n \left(\frac{\psi_i^{(\theta)}(\lambda)}{\hat{\mu}(\lambda)} - \frac{\hat{\theta}(\lambda)}{\hat{\mu}^2(\lambda)} \psi_i^{(\mu)}(\lambda) \right)^2.$$

Finally, the $(1 - \delta)$ one-sided upper confidence bound for the selected-set risk is

$$\text{UCB}^{\text{pt}}(\lambda; \delta) = \hat{r}(\lambda) + z_{1-\delta} \frac{\hat{\sigma}(\lambda)}{\sqrt{n}},$$

where $z_{1-\delta}$ is the $(1 - \delta)$ quantile of the standard normal distribution.

In practice, we apply this method with mild winsorization of the weights, capping the top 1% at the 99th percentile. When $\hat{\mu}(\lambda)$ is extremely small (e.g., $< 10/n$), we revert to the more conservative finite-sample upper bound described in Appendix A1.1.3.

A1.1.2 ASYMPTOTIC BOUNDS VIA NONPARAMETRIC BOOTSTRAP

As an alternative to the delta method, one may construct a nonparametric bootstrap upper confidence bound for $r(\lambda)$ by resampling the calibration data as outlined by Algorithm A1. Like the delta-method approximation, the bootstrap relies on large-sample asymptotics; therefore, if $\hat{\mu}(\lambda)$ is very small (e.g., $< 10/n$), we recommend reverting to the more conservative finite-sample upper bound described in Appendix A1.1.3.

Algorithm A1 Nonparametric bootstrap pointwise upper confidence bound.

input Pre-trained screening rule $A_\lambda : \mathcal{X} \mapsto \{0, 1\}$, calibration data $\mathcal{D}_{\text{cal}} = \{(X_i, \tilde{T}_i, E_i)\}_{i=1}^n$; fitted censoring model $\hat{G}(\cdot \mid X)$; number of bootstrap replicates B ; confidence level δ ; IPCW flavor **et** or **ft**.

- 1: **for** $b = 1, \dots, B$ **do**
- 2: Resample n calibration triples $\{(X_i^{*(b)}, \tilde{T}_i^{*(b)}, E_i^{*(b)})\}_{i=1}^n$ with replacement from \mathcal{D}_{cal} .
- 3: Recompute $\hat{\theta}^{*(b)}(\lambda)$ and $\hat{\mu}^{*(b)}(\lambda)$ using the same IPCW weights as in (5) or (6).
- 4: Form the bootstrap replicate $\hat{r}^{*(b)}(\lambda) = \hat{\theta}^{*(b)}(\lambda)/\hat{\mu}^{*(b)}(\lambda)$.
- 5: **end for**
- 6: Compute

$$\text{UCB}^{\text{boot}}(\lambda; \delta) = \text{Quantile}_{1-\delta}(\{\hat{r}^{*(b)}(\lambda)\}_{b=1}^B). \quad (\text{A14})$$

7: If $n_{\text{sel}}(\lambda) = \sum_i A_i(\lambda)$ is small (e.g., < 10), replace $\text{UCB}^{\text{boot}}(\lambda; \delta)$ with a conservative finite-sample bound.

output $(1 - \delta)$ pointwise upper confidence bound $\text{UCB}^{\text{boot}}(\lambda; \delta)$ for $r(\lambda)$.

A1.1.3 FINITE-SAMPLE BOUNDS VIA EMPIRICAL BERNSTEIN INEQUALITY

When the number of selected samples is very small, asymptotic approximations such as the delta-method or bootstrap can no longer be justified. In such cases, we can construct a finite-sample upper confidence bound for $r(\lambda) = \theta(\lambda)/\mu(\lambda)$ by combining an empirical-Bernstein concentration inequality for the numerator $\theta(\lambda)$ with an exact Clopper-Pearson lower bound for the selection fraction $\mu(\lambda)$.

For concreteness, we describe the event-time IPCW case; the fixed-time case is similar. Let $Z_i(\lambda) = A_\lambda(X_i) w_i^{\text{et}}$ and $w_i^{\text{et}} = 1/\tilde{G}(\tilde{T}_i^- \mid X_i)$, so that $\hat{\theta}(\lambda)$ can be written as $\hat{\theta}(\lambda) = \frac{1}{n} \sum_{i=1}^n Z_i$. Assume the weights are truncated at an upper bound M to stabilize the estimator; i.e., $w_i^{\text{et}} \leq M$ almost-surely. In practice, the constant M can be estimated empirically using the maximum of the weights in the calibration sample, after winsorization. The sample variance of the weighted contributions is given by

$$\hat{v}(\lambda) = \frac{1}{n-1} \sum_{i=1}^n (Z_i(\lambda) - \hat{\theta}(\lambda))^2.$$

The empirical-Bernstein inequality of Maurer and Pontil (2009) then implies that, with probability at least $1 - \delta/2$,

$$\theta(\lambda) \leq \hat{\theta}(\lambda) + \sqrt{\frac{2 \hat{v}(\lambda) \log(4/\delta)}{n}} + \frac{7M \log(4/\delta)}{3(n-1)}. \quad (\text{A15})$$

For the denominator, note that $n\hat{\mu}(\lambda) = \sum_{i=1}^n A_\lambda(X_i)$ follows a $\text{Binomial}(n, \mu(\lambda))$ distribution. An exact $(1 - \delta/2)$ lower confidence bound for $\mu(\lambda)$ is therefore

$$\hat{\mu}_{\text{low}}(\lambda; \delta) = \Psi_{\text{low}}(n, n\hat{\mu}(\lambda), \delta), \quad (\text{A16})$$

where $\Psi_{\text{low}}(n, k, \delta)$ is defined implicitly by

$$\text{pb} \text{inom}(k-1; n, \Psi_{\text{low}}(n, k, \delta)) = 1 - \delta,$$

and `pb`inom denotes the cumulative distribution function of the binomial distribution.

Combining the numerator bound (A15) and the denominator bound (A16) yields a finite-sample $(1 - \delta)$ one-sided upper confidence bound for the selected-set risk:

$$\text{UCB}^{\text{fs}}(\lambda; \delta) = \frac{\hat{\theta}_{\text{upp}}(\lambda; \delta/2)}{\hat{\mu}_{\text{low}}(\lambda; \delta/2)}, \quad (\text{A17})$$

where $\hat{\theta}_{\text{upp}}(\lambda; \delta/2)$ denotes the empirical-Bernstein upper bound in (A15). In practice, we recommend applying UCB^{fs} whenever the number of selected calibration samples $n_{\text{sel}}(\lambda) = \sum_i A_\lambda(X_i)$ is below 10.

A1.2 Greedy Pointwise Calibration

Algorithm A2 Greedy pointwise calibration

input Pre-trained screening rule $A_\lambda : \mathcal{X} \mapsto \{0, 1\}$ with parameter λ , calibration data $\mathcal{D}_{\text{cal}} = \{(X_i, \tilde{T}_i, E_i)\}_{i=1}^n$; censoring model $\hat{G}(\cdot | x)$; target risk level $\alpha \in (0, 1)$; confidence level $\delta \in (0, 1)$; grid $\Lambda = \{\lambda_1, \dots, \lambda_K\} \subset [0, 1]$; IPCW flavor **et** or **ft**; winsorization level τ (e.g., 1%).

- 1: Compute $\hat{\theta}(\lambda)$, $\hat{\mu}(\lambda)$ and $\hat{r}(\lambda) = \hat{\theta}(\lambda)/\hat{\mu}(\lambda)$ using winsorized IPCW as in (5) or (6).
- 2: Compute $\text{UCB}^{\text{pt}}(\lambda; \delta)$ (e.g., delta-method or finite-sample if $n_{\text{sel}}(\lambda) = \sum_i A_i(\lambda) \leq 10$).
- 3: Define the feasible set $\mathcal{F} \leftarrow \{\lambda \in \Lambda : \text{UCB}^{\text{pt}}(\lambda; \delta) \leq \alpha\}$.
- 4: If $\mathcal{F} = \emptyset$, set $\hat{\lambda} \leftarrow \text{NA}$. Otherwise choose $\hat{\lambda} \leftarrow \arg \max_{\lambda \in \mathcal{F}} n_{\text{sel}}(\lambda)$.

output Calibrated screening rule $A_{\hat{\lambda}}$.

A1.3 Conservative Uniform Calibration

The simplest way to obtain a UCB for $r(\lambda)$ that holds simultaneously with high probability across all $\lambda \in \Lambda$ is to apply the pointwise estimation methods from Section 3.1 with a Bonferroni correction. Specifically, the pointwise confidence level δ is replaced by the more conservative value δ/K , where $K = |\Lambda|$. The calibrated threshold is then chosen as

$$\hat{\lambda}_{\text{Bonferroni}} \in \arg \max_{\lambda \in \Lambda} \{ \hat{\mu}(\lambda) : \text{UCB}^{\text{pt}}(\lambda; \delta/|\Lambda|) \leq \alpha \},$$

where $\text{UCB}^{\text{pt}}(\lambda; \delta)$ represents a level- δ pointwise upper confidence bound for $r(\lambda)$, computed with any of the methods from Section 3.1. This Bonferroni correction guarantees $\mathbb{P}[r(\hat{\lambda}_{\text{Bonferroni}}) > \alpha] \leq \delta$, but tends to be overly conservative in practice, resulting in inefficient screening rules that tend to select fewer truly low-risk patients than would be feasible under less restrictive calibration. The source of this problem is that the Bonferroni correction does not account for the often strong dependencies between the estimation problems corresponding to different candidate thresholds $\lambda \in \Lambda$.

A less conservative alternative is the Gaussian multiplier (perturbation) approach, which constructs a joint confidence band by simulating correlated random fluctuations of the estimated risk across all $\lambda \in \Lambda = \{\lambda_1, \dots, \lambda_K\}$. This method builds on the same influence-function linearization that underlies the delta-method variance estimator (see Appendix A1.1 for additional details): for each individual i , we compute an estimated contribution $\phi_i(\lambda_k)$ that approximates the influence of observation i on $\hat{r}(\lambda_k)$, for all $k \in [K]$.

To approximate the joint sampling variability of $\hat{r}(\lambda_k)_{k=1}^K$, we repeatedly simulate random perturbations of these influence-function contributions. Let $\xi_i^{(b)} \sim \mathcal{N}(0, 1)$ denote independent standard normal random variables, sampled independently across bootstrap iterations $b = 1, \dots, B$ and individuals $i = 1, \dots, n$. For each iteration, we form the perturbed statistics

$$Z_k^{(b)} = \frac{1}{\sqrt{n}} \sum_{i=1}^n \xi_i^{(b)} \phi_i(\lambda_k), \quad \xi_i^{(b)} \stackrel{\text{i.i.d.}}{\sim} \mathcal{N}(0, 1),$$

and record the maximum fluctuation across thresholds, $T^{(b)} = \max_{k \leq K} |Z_k^{(b)}|$. The $(1 - \delta)$ quantile $q_{1-\delta}$ of $T^{(b)}_{b=1}^B$ provides a joint correction factor for the entire grid. This defines a

uniform half-width

$$h_{\text{GM}} = q_{1-\delta}/\sqrt{n}, \quad \text{UCB}^{\text{GM}}(\lambda_k; \delta) = \hat{r}(\lambda_k) + h_{\text{GM}}, \quad k = 1, \dots, K,$$

The calibrated threshold is then chosen as

$$\hat{\lambda}_{\text{GM}} \in \arg \max_{\lambda \in \Lambda} \left\{ \hat{\mu}(\lambda) : \text{UCB}^{\text{GM}}(\lambda; \delta) \leq \alpha \right\}.$$

Because all thresholds share the same simulated perturbations, this approach automatically captures the correlation between neighboring $\hat{r}(\lambda)$ values. As a result, the uniform confidence bounds are often substantially tighter than the Bonferroni bounds when $\hat{r}(\lambda)$ varies smoothly with λ , leading to more powerful screening rules.

Algorithm A3 Conservative uniform calibration

input Pre-trained screening rule $A_\lambda : \mathcal{X} \mapsto \{0, 1\}$ with parameter λ , calibration data $\mathcal{D}_{\text{cal}} = \{(X_i, \tilde{T}_i, E_i)\}_{i=1}^n$; censoring model $\hat{G}(\cdot \mid x)$; target risk level α ; confidence level δ ; grid $\Lambda = \{\lambda_1, \dots, \lambda_K\}$; IPCW flavor **et** or **ft**; band type **band** $\in \{\text{bonferroni}, \text{multiplier}\}$; number of draws B ; winsorization level τ .

- 1: Compute $\hat{\theta}(\lambda_k)$, $\hat{\mu}(\lambda_k)$, and $\hat{r}(\lambda_k) = \hat{\theta}(\lambda_k)/\hat{\mu}(\lambda_k)$ for all $\lambda_k \in \Lambda$ using winsorized IPCW as in (5) or (6).
- 2: Construct uniform upper confidence bounds on Λ :

- **bonferroni**: $\text{UCB}^{\text{uni}}(\lambda_k) \leftarrow \text{UCB}^{\text{pt}}(\lambda_k; \delta/K)$.
- **multiplier**: draw $\xi_i^{(b)} \sim \mathcal{N}(0, 1)$, compute $Z_k^{(b)} = n^{-1/2} \sum_i \xi_i^{(b)} \phi_i(\lambda_k)$, set $q_{1-\delta}$ to the $(1 - \delta)$ quantile of $T^{(b)} = \max_k |Z_k^{(b)}|$, and $\text{UCB}^{\text{uni}}(\lambda_k) = \hat{r}(\lambda_k) + q_{1-\delta}/\sqrt{n}$.

- 3: Define the feasible set $\mathcal{F} \leftarrow \{\lambda_k \in \Lambda : \text{UCB}^{\text{uni}}(\lambda_k; \delta) \leq \alpha\}$.

- 4: If $\mathcal{F} = \emptyset$, set $\hat{\lambda} \leftarrow \text{NA}$; otherwise $\hat{\lambda} \leftarrow \arg \max_{\lambda \in \mathcal{F}} n_{\text{sel}}(\lambda)$, where $n_{\text{sel}}(\lambda) = \sum_i A_i(\lambda)$.

output Calibrated screening rule $A_{\hat{\lambda}}$.

A1.4 Learn-then-Test (LTT) Calibration

Algorithm A4 Learn-Then-Test (LTT) calibration

input Pre-trained screening rule $A_\lambda : \mathcal{X} \mapsto \{0, 1\}$; calibration data $\mathcal{D}_{\text{cal}} = \{(X_i, \tilde{T}_i, E_i)\}_{i=1}^n$; survival model $\hat{S}(\cdot | x)$; censoring model $\hat{G}(\cdot | x)$; target risk level α ; confidence level δ ; IPCW flavor **et** or **ft**; winsorization level τ ; minimum selected count n_{\min} .

- 1: Compute calibration scores $s_i = \hat{S}(t_0 | X_i)$, and IPCW weights winsorized at level τ .
- 2: Define two anchor thresholds $\lambda_0^{(1)} = 1 - \alpha$ and $\lambda_0^{(2)} = 1 - \alpha/2$. For each anchor $l \in \{1, 2\}$, construct a decreasing sequence $\Lambda^{(l)} = \{\lambda_0^{(l)} > \lambda_1^{(l)} > \dots > \lambda_K^{(l)}\}$ by setting $\lambda_j^{(l)}$ to successive lower quantiles of $\{s_i\}$ below $\lambda_0^{(l)}$ (e.g., 95th, 92nd, 90th, ... percentiles).
- 3: Set per-path confidence level $\delta_* = \delta/2$.
- 4: **for** $l = 1, 2$ **do**
- 5: Initialize $\hat{\lambda}_{\text{LTT}}^{(l)} \leftarrow 1$.
- 6: **for** $\lambda \in \Lambda^{(l)}$ (in decreasing order) **do**
- 7: Compute pointwise upper confidence bound $\text{UCB}^{\text{pt}}(\lambda; \delta_*)$ for $r(\lambda)$.
- 8: **if** $\text{UCB}^{\text{pt}}(\lambda; \delta_*) \leq \alpha$ **then**
- 9: Set $\hat{\lambda}_{\text{LTT}}^{(l)} \leftarrow \lambda$.
- 10: **else**
- 11: **break**
- 12: **end if**
- 13: **end for**
- 14: **end for**
- 15: Set $\hat{\lambda}_{\text{LTT}} = \min\{\hat{\lambda}_{\text{LTT}}^{(1)}, \hat{\lambda}_{\text{LTT}}^{(2)}\}$.

output Calibrated screening rule $A_{\hat{\lambda}_{\text{LTT}}}$.

Appendix A2. Calibration via FDR Control with Conformal p -Values

A2.1 Proof of Proposition 1

Proof Let $R = |\hat{\mathcal{S}}|$ denote the number of selected test patients. For any test index $j \in [m]$, define $A(X_{n+j}) := \mathbb{I}[j \in \hat{\mathcal{S}}]$. Starting from the definition of FDR and applying tower property of conditional expectations, we immediately obtain:

$$\begin{aligned}
\text{FDR} &= \sum_{j=1}^m \sum_{k=1}^m \mathbb{E} \left[\frac{\mathbb{I}[T_{n+j} \leq t_0] A(X_{n+j})}{k} \mathbb{I}[R = k] \right] \\
&= \sum_{j=1}^m \sum_{k=1}^m \mathbb{E} \left[\frac{\mathbb{E}[\mathbb{I}[T_{n+j} \leq t_0] | A(X_{n+j}) = 1] A(X_{n+j})}{k} \mathbb{I}[R = k] \right] \\
&= \sum_{j=1}^m \sum_{k=1}^m \mathbb{E} \left[\frac{r(A; \mathcal{D}_{\text{cal}}) \cdot A(X_{n+j})}{k} \mathbb{I}[R = k] \right] \\
&= \sum_{k=1}^m \mathbb{E} \left[r(A; \mathcal{D}_{\text{cal}}) \frac{\sum_{j=1}^m A(X_{n+j})}{R} \mathbb{I}[R = k] \right] \\
&= \mathbb{E} \left[r(A; \mathcal{D}_{\text{cal}}) \cdot \sum_{k=1}^m \mathbb{P}[R = k | \mathcal{D}_{\text{cal}}] \right] \\
&= \mathbb{E}[r(A; \mathcal{D}_{\text{cal}}) \mathbb{P}[R > 0 | \mathcal{D}_{\text{cal}}]].
\end{aligned}$$

■

A2.2 Additional Implementation Details

The offset parameter γ used by Algorithm 1 to compute $s_i = \hat{S}(\tilde{T}_i + \gamma | X_i)$ and $s_{n+j} = \hat{S}(t_0 + \gamma | X_{n+j})$ should be tuned on a tuning data set *independent* of the calibration data in order to maximize power without invalidating any guarantees.

In practice, we tune γ as described below and summarized by Algorithm A5. First, define a grid Γ of candidate values (e.g., $\{0\}$ together with several quantiles of the observed event times). Then, repeatedly split the training data (assumed independent of the calibration data) into three subsets: a tuning-training set for model fitting, a tuning-calibration set for conformal calibration, and a tuning-test set for evaluation. On each split, fit smaller survival and censoring models using the tuning-training subset, then apply Algorithm 1 for each candidate value of γ using the tuning-calibration and tuning-test subsets in place of the true calibration and test sets. Measure performance on the tuning-test set either by (i) the yield at level α , or (ii) in lower-power settings, by the smoother Fisher combination statistic $-2 \sum_i \log \hat{p}_i$, where \hat{p}_i denote the conformal p -values for the tuning-test set. In our experiments, we adopt the Fisher criterion by default and set the stability threshold for the optional abstention rule to $\nu = 0.9$ when estimating $\mathbb{P}(R > 0)$ via bootstrap. Then, we average the performance score across several random splits, and select

$$\gamma^* = \arg \max_{\gamma \in \Gamma} \text{AverageScore}(\gamma).$$

Algorithm A5 Cross-validation to tune the offset parameter γ for Algorithm 1

input Tuning dataset $\mathcal{D}_{\text{tune}} = \{(X_i, \tilde{T}_i, E_i)\}_{i=1}^N$ (independent of final calibration data); pre-fitted survival model $\hat{S}(\cdot | x)$ and censoring model $\hat{G}(\cdot | x)$; horizon t_0 ; target level α ; candidate grid Γ ; number of repetitions R ; split fractions $(\pi_{\text{cal}}, \pi_{\text{test}})$; evaluation criterion $\in \{\text{BH}, \text{Fisher}\}$.

- 1: **for** $r = 1$ to R **do**
- 2: Randomly split $\mathcal{D}_{\text{tune}}$ into disjoint subsets $D_{\text{tune}}^{\text{train}}$, $D_{\text{tune}}^{\text{cal}}$, and $D_{\text{tune}}^{\text{test}}$ according to fractions $(1 - \pi_{\text{cal}} - \pi_{\text{test}}, \pi_{\text{cal}}, \pi_{\text{test}})$.
- 3: Optionally refit smaller models \hat{S}_r, \hat{G}_r on $D_{\text{tune}}^{\text{train}}$ (otherwise use \hat{S}, \hat{G}).
- 4: **for** each $\gamma \in \Gamma$ **do**
- 5: Apply Algorithm 1 using calibration set $D_{\text{tune}}^{\text{cal}}$, test set $D_{\text{tune}}^{\text{test}}$, and offset γ , obtaining conformal p -values $\{\hat{p}_j\}$.
- 6: Compute the performance score $J_r(\gamma)$: number of BH rejections at level α , or Fisher statistic $J_r(\gamma) = -2 \sum_j \log \hat{p}_j$.
- 7: **end for**
- 8: **end for**
- 9: Aggregate scores $\bar{J}(\gamma) = R^{-1} \sum_{r=1}^R J_r(\gamma)$.
- 10: Select $\gamma^* = \arg \max_{\gamma \in \Gamma} \bar{J}(\gamma)$ (break ties by smallest γ).

output Tuned offset γ^* .

Finally, fix $\gamma = \gamma^*$ and run Algorithm 1 on the actual calibration and test sets. For computational efficiency, we can precompute $\hat{S}(\cdot | X)$ on a fine time grid and use interpolation to evaluate $\hat{S}(\tilde{T}_i + \gamma | X_i)$ and $\hat{S}(t_0 + \gamma | X_i)$ for all $\gamma \in \Gamma$, avoiding repeated model calls.

Appendix A3. Additional Numerical Results

A3.1 Experiments with Simulated Data

Table A1: Detailed numerical summary of results corresponding to Figure 1. Each entry shows the mean and (in parenthesis) two standard errors across repeated trials. Each entry shows the mean and uncertainty (2 SE) across repeated trials. Values in bold indicate the method selecting the most patients at each time (among those with valid survival rate). Conditional results are not evaluated if selections occur in fewer than 10% of experiments.

Method	Yield	Survival	Survival (cond.)	$P(S > 0)$
Horizon: 2 months				
Oracle	841 (3.69)	1 (0.00)	1 (0.00)	1 (0.00)
Model	760 (8.35)	0.91 (0.00)	0.91 (0.00)	1.00 (0.00)
FDR-Conformal	770 (18.01)	0.90 (0.00)	0.90 (0.00)	1.00 (0.00)
HP-Greedy	685 (30.88)	0.91 (0.00)	0.91 (0.00)	0.99 (0.02)
HP-Uniform	71 (27.39)	0.98 (0.01)	0.95 (0.01)	0.47 (0.10)
HP-LTT	629 (46.07)	0.92 (0.01)	0.91 (0.00)	0.93 (0.05)
Horizon: 3 months				
Oracle	538 (4.16)	1 (0.00)	1 (0.00)	1 (0.00)
Model	324 (14.95)	0.91 (0.00)	0.91 (0.00)	1.00 (0.00)
FDR-Conformal	355 (39.78)	0.92 (0.01)	0.90 (0.00)	0.84 (0.07)
HP-Greedy	277 (37.31)	0.92 (0.01)	0.91 (0.01)	0.91 (0.06)
HP-Uniform	19 (8.15)	0.98 (0.01)	0.93 (0.01)	0.32 (0.09)
HP-LTT	150 (37.34)	0.96 (0.01)	0.91 (0.00)	0.50 (0.10)
Horizon: 6 months				
Oracle	25 (1.17)	1 (0.01)	1 (0.01)	1 (0.00)
Model	0 (0.00)	1.00 (0.00)	NA	0.00 (0.00)
FDR-Conformal	5 (3.76)	0.99 (0.01)	NA	0.07 (0.05)
HP-Greedy	11 (5.49)	0.95 (0.02)	0.82 (0.02)	0.27 (0.09)
HP-Uniform	3 (1.46)	0.97 (0.02)	0.82 (0.02)	0.16 (0.07)
HP-LTT	3 (1.61)	0.97 (0.02)	0.81 (0.02)	0.16 (0.07)
Horizon: 9 months				
Oracle	0 (0.00)	1 (0.00)	NA	0 (0.00)
Model	0 (0.00)	1.00 (0.00)	NA	0.00 (0.00)
FDR-Conformal	0 (0.00)	1.00 (0.00)	NA	0.00 (0.00)
HP-Greedy	2 (1.13)	0.97 (0.02)	0.77 (0.03)	0.15 (0.07)
HP-Uniform	0 (0.37)	0.99 (0.01)	NA	0.03 (0.03)
HP-LTT	2 (0.81)	0.97 (0.02)	0.76 (0.03)	0.14 (0.07)

Table A2: Detailed numerical summary of results corresponding to Figure 3. Each entry shows the mean and (in parenthesis) two standard errors across repeated trials. Each entry shows the mean and uncertainty (2 SE) across repeated trials. Values in bold indicate the method selecting the most patients at each time (among those with valid survival rate). Values highlighted in red denote survival rates significantly below the 90% target.

Method	Yield	Survival	Survival (cond.)	$P(S > 0)$
Horizon: 2 months				
Oracle	841 (5.12)	1 (0.00)	1 (0.00)	1 (0.00)
Model	859 (7.72)	0.89 (0.00)	0.89 (0.00)	1.00 (0.00)
FDR-Conformal	630 (62.51)	0.90 (0.01)	0.90 (0.00)	0.96 (0.06)
HP-Greedy	373 (78.16)	0.93 (0.01)	0.92 (0.01)	0.96 (0.06)
HP-Uniform	21 (17.41)	0.98 (0.01)	0.95 (0.01)	0.41 (0.15)
HP-LTT	276 (88.31)	0.95 (0.01)	0.91 (0.01)	0.52 (0.15)
Horizon: 3 months				
Oracle	536 (5.70)	1 (0.00)	1 (0.00)	1 (0.00)
Model	705 (9.55)	0.85 (0.00)	0.85 (0.00)	1.00 (0.00)
FDR-Conformal	157 (44.25)	0.93 (0.02)	0.89 (0.01)	0.67 (0.14)
HP-Greedy	49 (27.37)	0.97 (0.01)	0.92 (0.01)	0.44 (0.14)
HP-Uniform	6 (3.69)	0.98 (0.01)	0.94 (0.02)	0.31 (0.14)
HP-LTT	8 (11.54)	0.99 (0.01)	NA	0.04 (0.06)
Horizon: 6 months				
Oracle	26 (1.81)	1 (0.02)	1 (0.02)	1 (0.00)
Model	438 (8.81)	0.76 (0.01)	0.76 (0.01)	1.00 (0.00)
FDR-Conformal	4 (3.68)	0.98 (0.02)	0.82 (0.01)	0.10 (0.09)
HP-Greedy	3 (4.06)	0.98 (0.02)	NA	0.08 (0.08)
HP-Uniform	1 (1.96)	0.98 (0.02)	NA	0.06 (0.07)
HP-LTT	2 (3.43)	1.00 (0.01)	NA	0.02 (0.04)
Horizon: 9 months				
Oracle	0 (0.00)	1 (0.00)	NA	0 (0.00)
Model	304 (7.73)	0.68 (0.01)	0.68 (0.01)	1.00 (0.00)
FDR-Conformal	2 (2.09)	0.98 (0.02)	NA	0.06 (0.07)
HP-Greedy	1 (1.20)	0.97 (0.03)	NA	0.06 (0.07)
HP-Uniform	0 (0.28)	0.99 (0.02)	NA	0.02 (0.04)
HP-LTT	0 (0.00)	1.00 (0.00)	NA	0.00 (0.00)

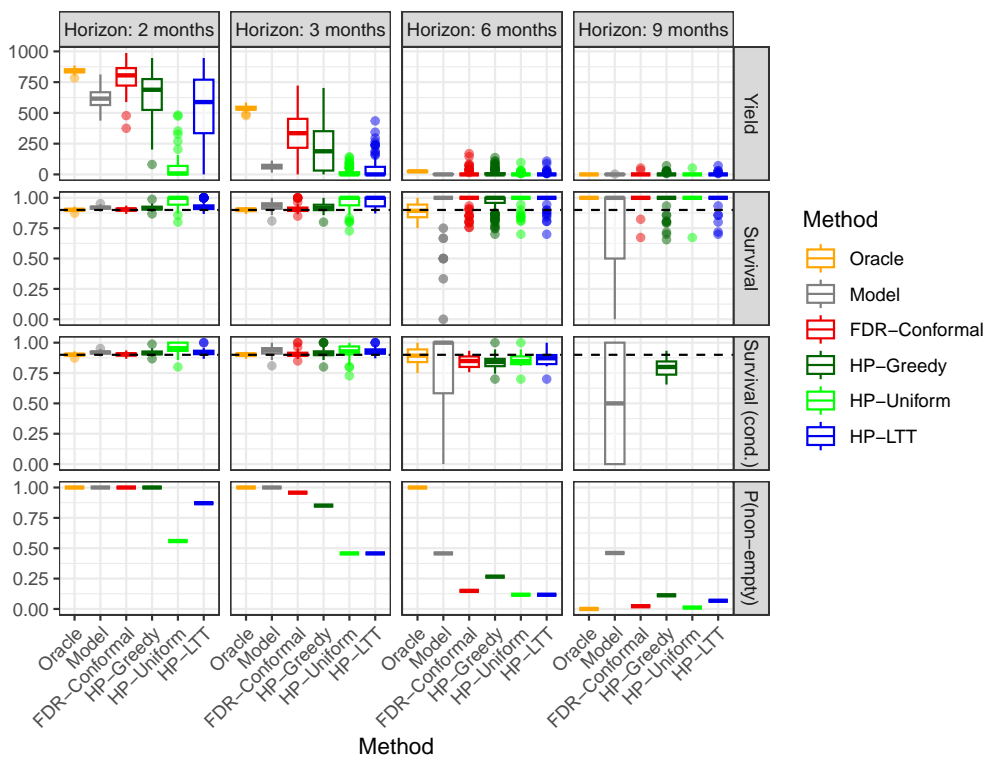


Figure A1: Summary of low-risk screening results obtained by applying different calibration methods to semi-synthetic oncology data simulated using a random forest generative model, at different screening horizons. All methods use the same mis-specified Cox survival model. Other details as in Figure 1.

Table A3: Detailed numerical summary of results corresponding to Figure A1. Each entry shows the mean and (in parenthesis) two standard errors across repeated trials. Each entry shows the mean and uncertainty (2 SE) across repeated trials. Values in bold indicate the method selecting the most patients at each time (among those with valid survival rate). Values highlighted in red denote survival rates significantly below the 90% target.

Method	Yield	Survival	Survival (cond.)	$P(S > 0)$
Horizon: 2 months				
Oracle	841 (3.75)	1 (0.00)	1 (0.00)	1 (0.00)
Model	612 (15.86)	0.92 (0.00)	0.92 (0.00)	1.00 (0.00)
FDR-Conformal	787 (22.40)	0.90 (0.00)	0.90 (0.00)	1.00 (0.00)
HP-Greedy	636 (37.58)	0.92 (0.00)	0.92 (0.00)	1.00 (0.00)
HP-Uniform	51 (19.69)	0.97 (0.01)	0.95 (0.01)	0.56 (0.10)
HP-LTT	520 (59.32)	0.93 (0.01)	0.92 (0.00)	0.87 (0.07)
Horizon: 3 months				
Oracle	538 (4.28)	1 (0.00)	1 (0.00)	1 (0.00)
Model	63 (4.74)	0.93 (0.01)	0.93 (0.01)	1.00 (0.00)
FDR-Conformal	340 (38.85)	0.91 (0.01)	0.91 (0.01)	0.96 (0.04)
HP-Greedy	219 (38.70)	0.93 (0.01)	0.91 (0.01)	0.85 (0.07)
HP-Uniform	18 (6.72)	0.97 (0.01)	0.93 (0.01)	0.46 (0.10)
HP-LTT	50 (17.99)	0.97 (0.01)	0.93 (0.01)	0.46 (0.10)
Horizon: 6 months				
Oracle	25 (1.21)	1 (0.01)	1 (0.01)	1 (0.00)
Model	1 (0.28)	0.91 (0.04)	0.81 (0.06)	0.46 (0.10)
FDR-Conformal	9 (5.80)	0.98 (0.01)	0.84 (0.01)	0.15 (0.07)
HP-Greedy	13 (5.72)	0.96 (0.02)	0.84 (0.01)	0.27 (0.09)
HP-Uniform	3 (2.37)	0.98 (0.01)	0.86 (0.02)	0.12 (0.07)
HP-LTT	4 (3.18)	0.98 (0.01)	0.86 (0.02)	0.12 (0.07)
Horizon: 9 months				
Oracle	0 (0.00)	1 (0.00)	NA	0 (0.00)
Model	1 (0.15)	0.78 (0.08)	0.52 (0.10)	0.46 (0.11)
FDR-Conformal	1 (1.39)	0.99 (0.01)	NA	0.02 (0.03)
HP-Greedy	3 (2.10)	0.98 (0.02)	0.79 (0.02)	0.11 (0.07)
HP-Uniform	1 (1.17)	1.00 (0.01)	NA	0.01 (0.02)
HP-LTT	2 (1.86)	0.99 (0.01)	NA	0.07 (0.05)

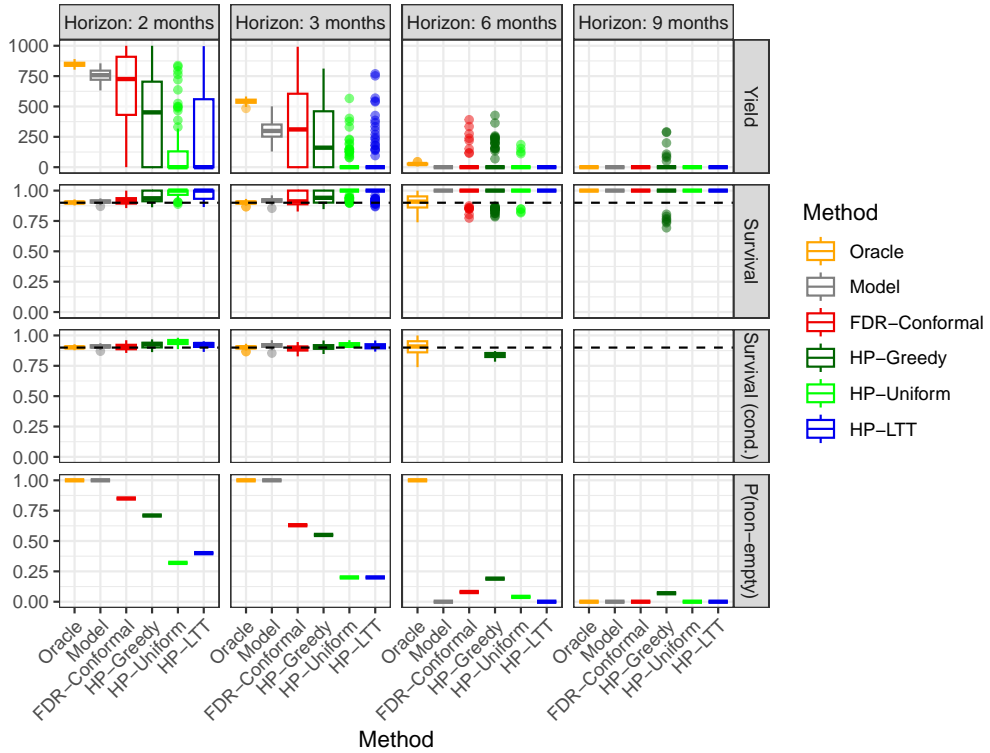


Figure A2: Summary of low-risk screening results obtained by applying different methods to semi-synthetic oncology data simulated from a grf generative survival model, at different screening horizons. Calibration sample size 100. Other details as in Figure 1.

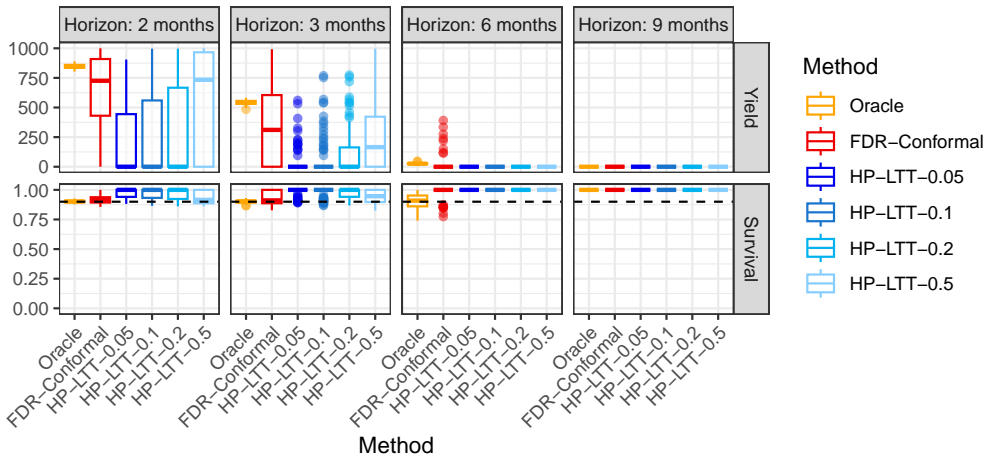


Figure A3: Summary of low-risk screening results on semi-synthetic oncology data. As in Figure A3, the LTT calibration method is applied at different confidence levels δ , ranging from $\delta = 0.05$ (more conservative) to $\delta = 0.5$ (more liberal). Here, the calibration sample size is 100 instead of 1000.

Table A4: Detailed numerical summary of results corresponding to Figure A2. Each entry shows the mean and (in parenthesis) two standard errors across repeated trials. Each entry shows the mean and uncertainty (2 SE) across repeated trials. Values in bold indicate the method selecting the most patients at each time (among those with valid survival rate). Values highlighted in red denote survival rates significantly below the 90% target.

Method	Yield	Survival	Survival (cond.)	$P(S > 0)$
Horizon: 2 months				
Oracle	847 (3.54)	1 (0.00)	1 (0.00)	1 (0.00)
Model	758 (10.09)	0.91 (0.00)	0.91 (0.00)	1.00 (0.00)
FDR-Conformal	628 (67.50)	0.92 (0.01)	0.91 (0.00)	0.85 (0.07)
HP-Greedy	419 (69.35)	0.94 (0.01)	0.92 (0.01)	0.71 (0.09)
HP-Uniform	110 (42.39)	0.98 (0.01)	0.94 (0.00)	0.32 (0.09)
HP-LTT	255 (66.33)	0.97 (0.01)	0.92 (0.00)	0.40 (0.10)
Horizon: 3 months				
Oracle	543 (4.08)	1 (0.00)	1 (0.00)	1 (0.00)
Model	299 (15.23)	0.92 (0.00)	0.92 (0.00)	1.00 (0.00)
FDR-Conformal	329 (62.00)	0.93 (0.01)	0.89 (0.01)	0.63 (0.10)
HP-Greedy	233 (52.32)	0.95 (0.01)	0.90 (0.01)	0.55 (0.10)
HP-Uniform	40 (19.46)	0.98 (0.01)	0.92 (0.00)	0.20 (0.08)
HP-LTT	68 (32.61)	0.98 (0.01)	0.91 (0.00)	0.20 (0.08)
Horizon: 6 months				
Oracle	26 (1.19)	1 (0.01)	1 (0.01)	1 (0.00)
Model	0 (0.00)	1.00 (0.00)	NA	0.00 (0.00)
FDR-Conformal	18 (13.66)	0.99 (0.01)	NA	0.08 (0.05)
HP-Greedy	41 (18.31)	0.97 (0.01)	0.84 (0.01)	0.19 (0.08)
HP-Uniform	6 (5.80)	0.99 (0.01)	NA	0.04 (0.04)
HP-LTT	0 (0.00)	1.00 (0.00)	NA	0.00 (0.00)
Horizon: 9 months				
Oracle	0 (0.00)	1 (0.00)	NA	0 (0.00)
Model	0 (0.00)	1.00 (0.00)	NA	0.00 (0.00)
FDR-Conformal	0 (0.00)	1.00 (0.00)	NA	0.00 (0.00)
HP-Greedy	11 (9.51)	0.98 (0.01)	NA	0.07 (0.05)
HP-Uniform	0 (0.00)	1.00 (0.00)	NA	0.00 (0.00)
HP-LTT	0 (0.00)	1.00 (0.00)	NA	0.00 (0.00)

A3.2 Experiments with Real Data

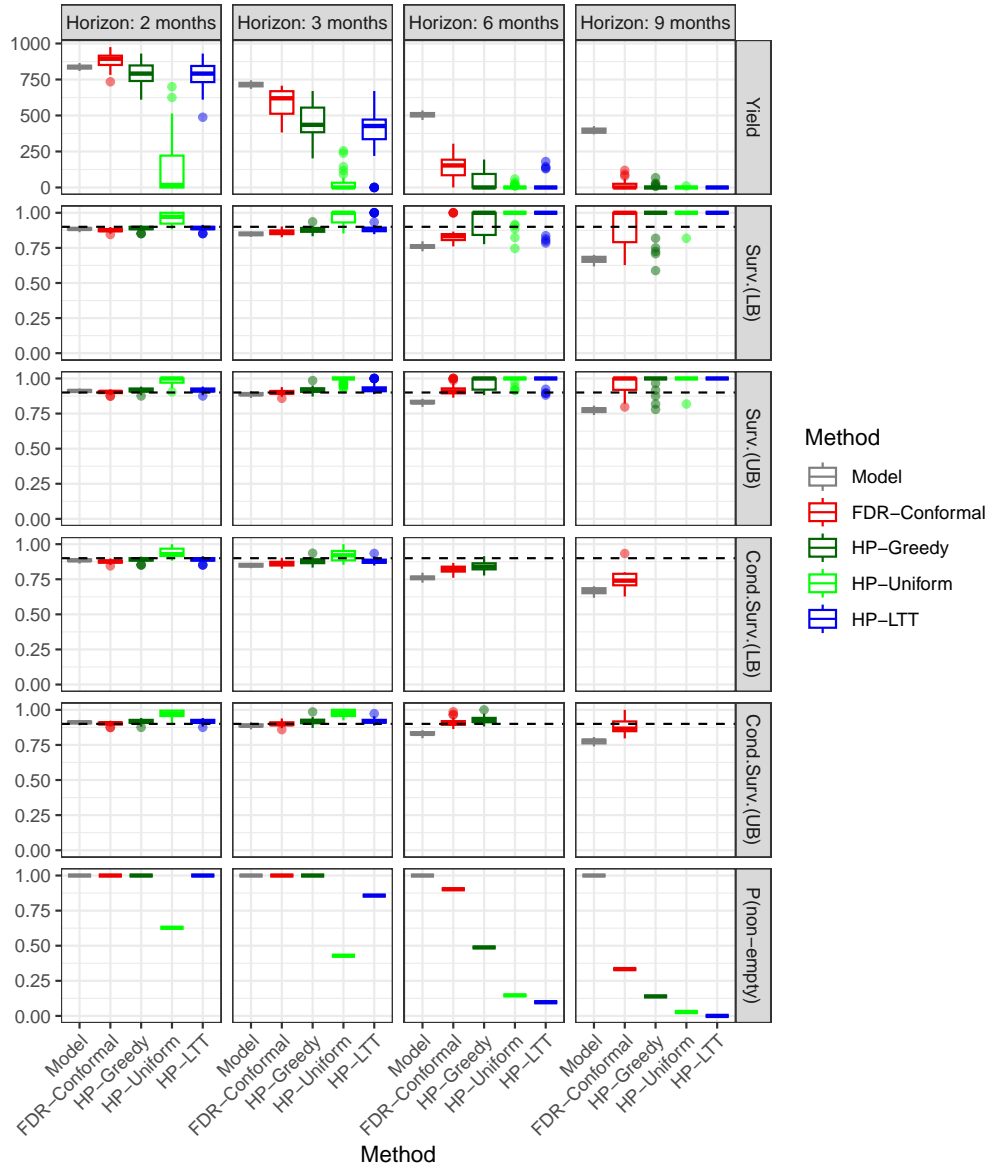


Figure A4: Summary of low-risk screening results obtained by applying different methods to real oncology data, at different screening horizons, using a gradient boosting survival model. Other details as in Table 1.

Table A5: Summary of low-risk screening results obtained by applying different methods to real oncology data, at different screening horizons, using a Cox survival model. Other details are as in Table 1.

Method	Yield	Surv.(LB)	Surv.(UB)	C.Surv.(LB)	C.Surv.(UB)	P(S > 0)
Horizon: 2 months						
Model	823 (4.21)	0.89 (0.00)	0.92 (0.00)	0.89 (0.00)	0.92 (0.00)	1.00 (0.00)
FDR-Conformal	917 (7.87)	0.87 (0.00)	0.90 (0.00)	0.87 (0.00)	0.90 (0.00)	1.00 (0.00)
HP-Greedy	860 (11.83)	0.89 (0.00)	0.91 (0.00)	0.89 (0.00)	0.91 (0.00)	1.00 (0.00)
HP-Uniform	186 (65.31)	0.97 (0.01)	0.98 (0.01)	0.93 (0.01)	0.96 (0.01)	0.42 (0.12)
HP-LTT	860 (11.79)	0.89 (0.00)	0.91 (0.00)	0.89 (0.00)	0.91 (0.00)	1.00 (0.00)
Horizon: 3 months						
Model	390 (4.17)	0.91 (0.00)	0.95 (0.00)	0.91 (0.00)	0.95 (0.00)	1.00 (0.00)
FDR-Conformal	682 (13.55)	0.86 (0.00)	0.90 (0.00)	0.86 (0.00)	0.90 (0.00)	1.00 (0.00)
HP-Greedy	608 (20.18)	0.88 (0.00)	0.91 (0.00)	0.88 (0.00)	0.91 (0.00)	1.00 (0.00)
HP-Uniform	87 (34.33)	0.97 (0.01)	0.98 (0.01)	0.92 (0.01)	0.96 (0.01)	0.42 (0.11)
HP-LTT	583 (28.84)	0.88 (0.01)	0.92 (0.01)	0.88 (0.01)	0.92 (0.01)	1.00 (0.00)
Horizon: 6 months						
Model	32 (1.81)	0.88 (0.01)	0.96 (0.01)	0.88 (0.01)	0.96 (0.01)	1.00 (0.00)
FDR-Conformal	211 (22.79)	0.86 (0.01)	0.92 (0.01)	0.84 (0.01)	0.91 (0.01)	0.91 (0.07)
HP-Greedy	136 (26.94)	0.90 (0.02)	0.94 (0.01)	0.85 (0.01)	0.92 (0.01)	0.72 (0.10)
HP-Uniform	14 (6.98)	0.97 (0.01)	0.99 (0.01)	0.89 (0.01)	0.95 (0.01)	0.28 (0.10)
HP-LTT	43 (20.46)	0.96 (0.02)	0.98 (0.01)	0.87 (0.01)	0.93 (0.01)	0.32 (0.11)
Horizon: 9 months						
Model	6 (0.85)	0.87 (0.03)	0.97 (0.02)	0.86 (0.03)	0.96 (0.02)	0.92 (0.06)
FDR-Conformal	35 (9.34)	0.88 (0.03)	0.94 (0.01)	0.80 (0.01)	0.90 (0.01)	0.59 (0.11)
HP-Greedy	21 (8.69)	0.92 (0.02)	0.97 (0.01)	0.80 (0.01)	0.92 (0.01)	0.39 (0.11)
HP-Uniform	3 (2.12)	0.98 (0.01)	0.99 (0.01)	0.82 (0.02)	0.92 (0.01)	0.11 (0.07)
HP-LTT	7 (5.01)	0.96 (0.02)	0.98 (0.01)	0.80 (0.02)	0.93 (0.01)	0.22 (0.10)

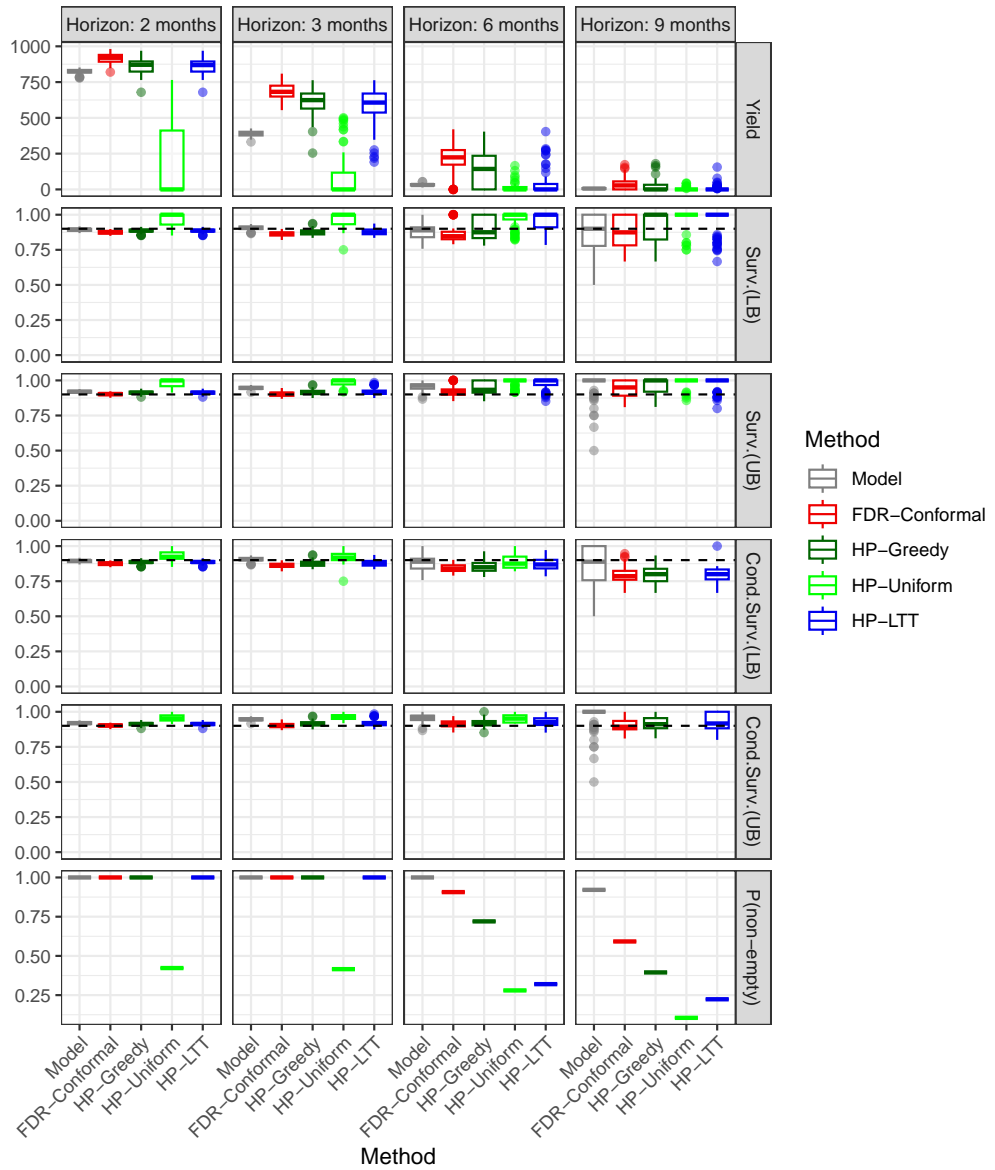


Figure A5: Summary of low-risk screening results obtained by applying different methods to real oncology data, at different screening horizons, using a Cox survival model. Other details as in Figure A4.

Table A6: Summary of low-risk screening results obtained by applying different methods to real oncology data, at different screening horizons, using a generalized random forest survival model. Other details are as in Table 1.

Method	Yield	Surv.(LB)	Surv.(UB)	C.Surv.(LB)	C.Surv.(UB)	P(S > 0)
Horizon: 2 months						
Model	834 (4.43)	0.89 (0.00)	0.92 (0.00)	0.89 (0.00)	0.92 (0.00)	1.00 (0.00)
FDR-Conformal	868 (11.11)	0.88 (0.00)	0.91 (0.00)	0.88 (0.00)	0.91 (0.00)	1.00 (0.00)
HP-Greedy	840 (13.93)	0.89 (0.00)	0.91 (0.00)	0.89 (0.00)	0.91 (0.00)	1.00 (0.00)
HP-Uniform	351 (61.33)	0.95 (0.01)	0.96 (0.01)	0.93 (0.01)	0.95 (0.00)	0.72 (0.09)
HP-LTT	838 (14.75)	0.89 (0.00)	0.91 (0.00)	0.89 (0.00)	0.91 (0.00)	1.00 (0.00)
Horizon: 3 months						
Model	509 (4.56)	0.89 (0.00)	0.92 (0.00)	0.89 (0.00)	0.92 (0.00)	1.00 (0.00)
FDR-Conformal	603 (18.39)	0.87 (0.00)	0.91 (0.00)	0.87 (0.00)	0.91 (0.00)	1.00 (0.00)
HP-Greedy	560 (21.41)	0.88 (0.00)	0.92 (0.00)	0.88 (0.00)	0.92 (0.00)	1.00 (0.00)
HP-Uniform	160 (34.52)	0.95 (0.01)	0.97 (0.01)	0.92 (0.01)	0.96 (0.01)	0.71 (0.09)
HP-LTT	538 (26.77)	0.88 (0.01)	0.92 (0.00)	0.88 (0.01)	0.92 (0.00)	0.99 (0.02)
Horizon: 6 months						
Model	13 (1.31)	0.93 (0.02)	0.98 (0.01)	0.93 (0.02)	0.98 (0.01)	1.00 (0.00)
FDR-Conformal	82 (18.14)	0.91 (0.02)	0.95 (0.01)	0.85 (0.01)	0.92 (0.01)	0.60 (0.10)
HP-Greedy	130 (18.48)	0.88 (0.01)	0.94 (0.01)	0.87 (0.01)	0.93 (0.01)	0.92 (0.06)
HP-Uniform	19 (7.91)	0.96 (0.01)	0.98 (0.01)	0.90 (0.01)	0.95 (0.01)	0.37 (0.10)
HP-LTT	33 (15.38)	0.96 (0.01)	0.98 (0.01)	0.89 (0.01)	0.94 (0.01)	0.36 (0.10)
Horizon: 9 months						
Model	0 (0.00)	1.00 (0.00)	1.00 (0.00)	NA	NA	0.00 (0.00)
FDR-Conformal	2 (2.19)	0.99 (0.01)	1.00 (0.00)	NA	NA	0.04 (0.04)
HP-Greedy	28 (8.51)	0.92 (0.02)	0.95 (0.01)	0.81 (0.01)	0.90 (0.01)	0.43 (0.10)
HP-Uniform	3 (2.18)	0.98 (0.01)	0.99 (0.01)	0.82 (0.02)	0.92 (0.01)	0.13 (0.07)
HP-LTT	6 (3.52)	0.97 (0.01)	0.98 (0.01)	0.83 (0.01)	0.90 (0.01)	0.19 (0.08)

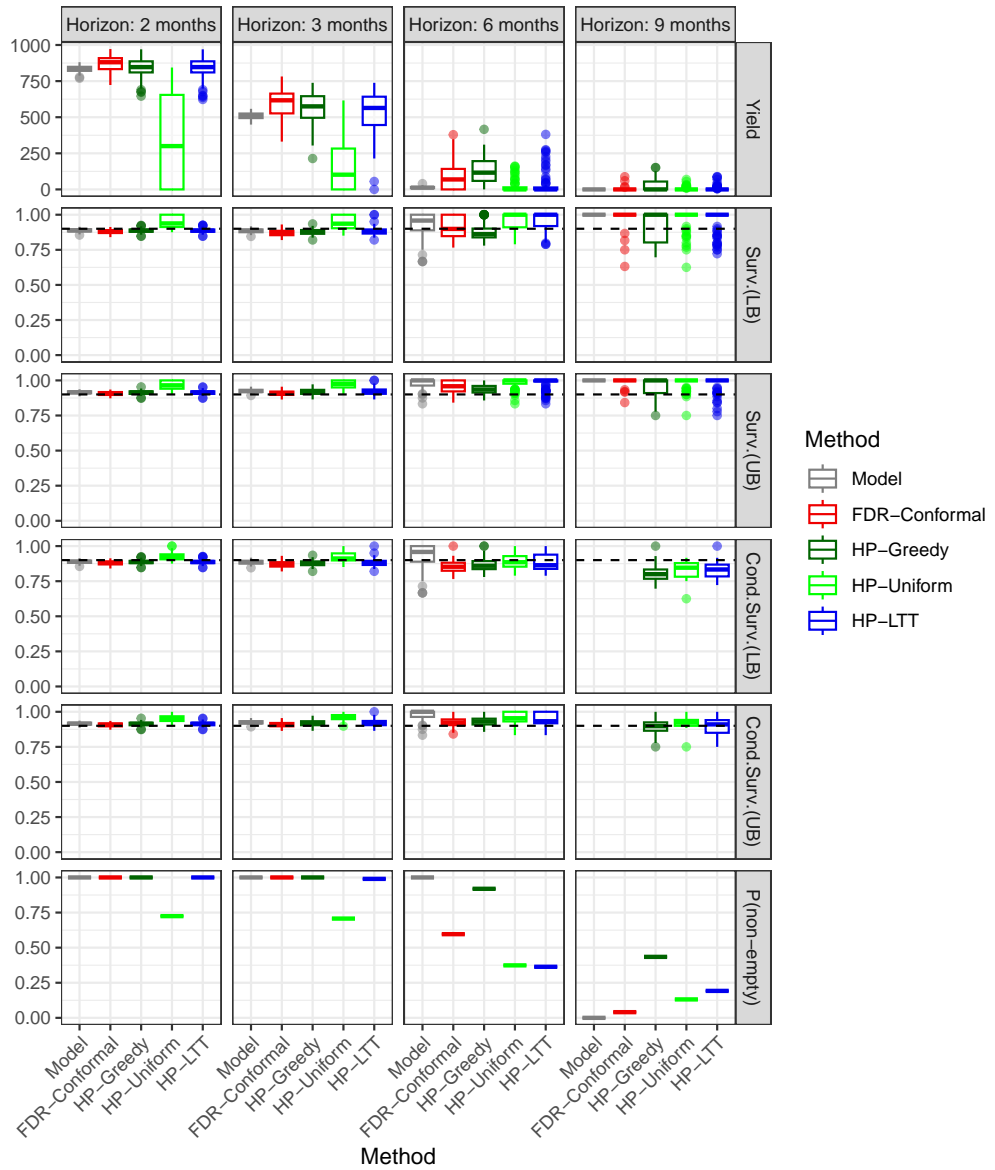


Figure A6: Summary of low-risk screening results obtained by applying different methods to real oncology data, at different screening horizons, using a generalized random forest survival model. Other details as in Figure A4.

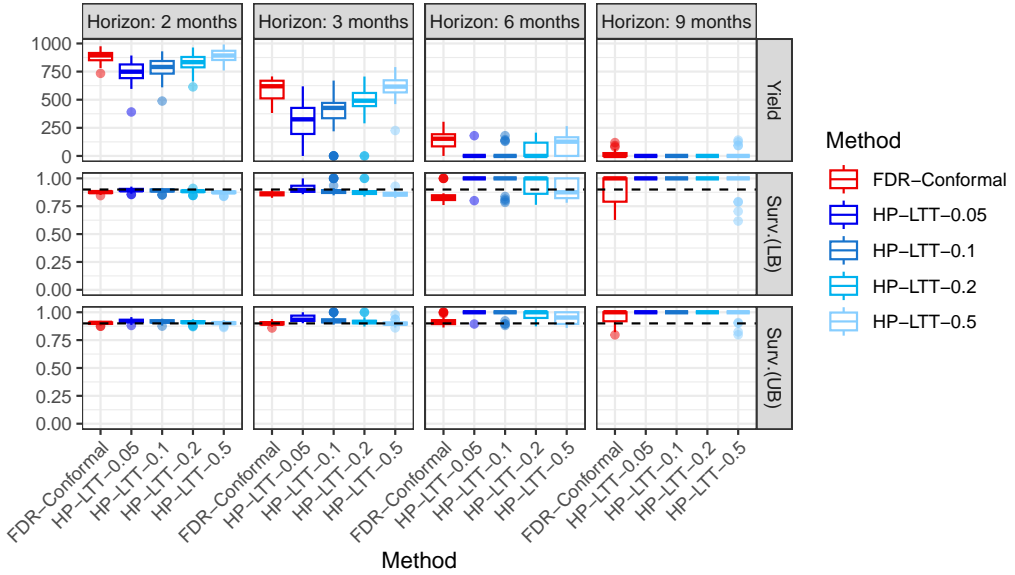


Figure A7: Summary of low-risk screening results on real oncology data, using a gradient boosting survival model as in Figure A4. Here, the LTT calibration method is applied at different confidence levels δ , ranging from $\delta = 0.05$ (more conservative) to $\delta = 0.5$ (more liberal).

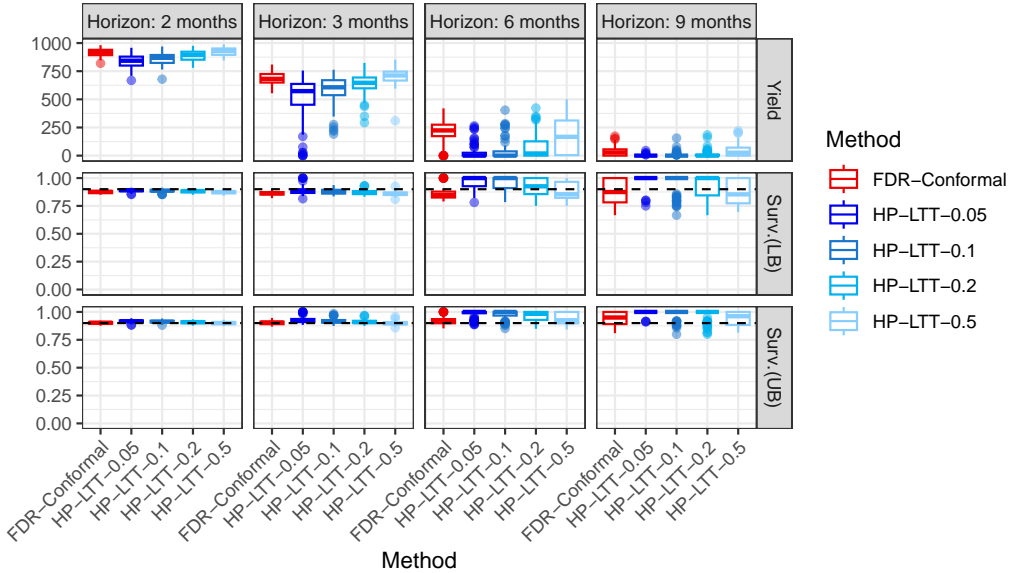


Figure A8: Summary of low-risk screening results on real oncology data, using a Cox survival model as in Figure A5. Here, the LTT calibration method is applied at different confidence levels δ , ranging from $\delta = 0.05$ (more conservative) to $\delta = 0.5$ (more liberal).

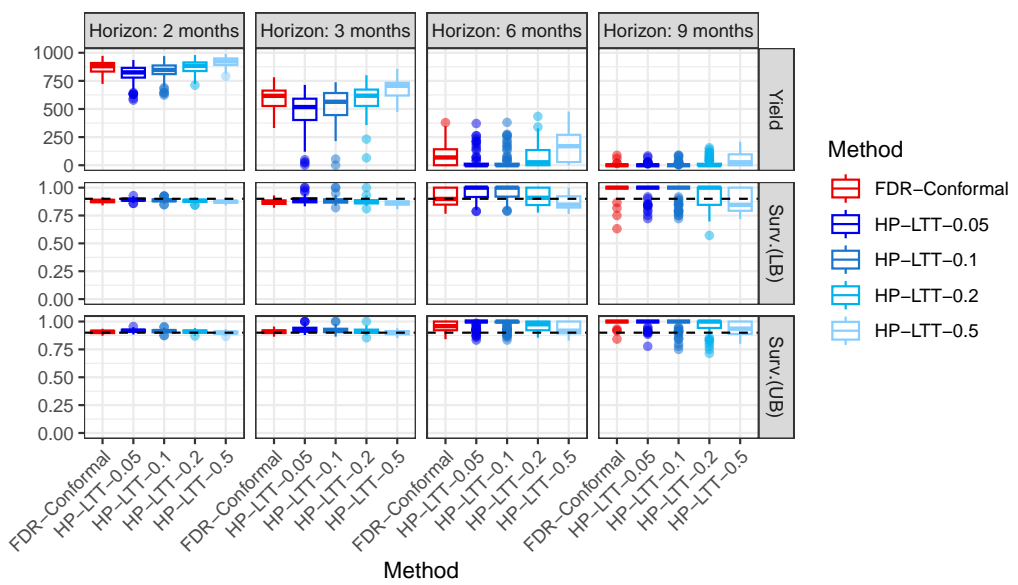


Figure A9: Summary of low-risk screening results on real oncology data, using a generalized random forest survival model as in Figure A6. Here, the LTT calibration method is applied at different confidence levels δ , ranging from $\delta = 0.05$ (more conservative) to $\delta = 0.5$ (more liberal).